

A TIME-DELAY IN THE ACTIVATOR KINETICS ENHANCES THE STABILITY OF A SPIKE SOLUTION TO THE GIERER-MEINHARDT MODEL

NABIL T. FADAI*, MICHAEL J. WARD†, AND JUNCHENG WEI‡

Abstract. We study the spectrum of a new class of nonlocal eigenvalue problems (NLEPs) that characterize the linear stability properties of localized spike solutions to the singularly perturbed two-component Gierer-Meinhardt (GM) reaction-diffusion (RD) system with a fixed time-delay T in only the nonlinear autocatalytic activator kinetics. Our analysis of this model is motivated by the computational study of Seirin Lee et al. [Bull. Math. Bio., **72**(8), (2010)] on the effect of gene expression time delays on spatial patterning for both the GM and some related RD models. For various limiting forms of the GM model, we show from a numerical study of the associated NLEP, together with an analytical scaling law analysis valid for large delay T , that a time-delay in only the activator kinetics is stabilizing in the sense that there is a wider region of parameter space where the spike solution is linearly stable than when there is no time delay. This enhanced stability behavior with a delayed activator kinetics is in marked contrast to the de-stabilizing effect on spike solutions of having a time-delay in both the activator and inhibitor kinetics. Numerical results computed from the RD system with delayed activator kinetics are used to validate the theory for the 1-D case.

1. Introduction. For activator-inhibitor two-component reaction-diffusion (RD) systems, it is a well-known result, originating from Turing [21], that a small perturbation of a spatially uniform steady-state solution can become unstable when the diffusivity ratio is large enough. This initial instability then leads to the generation of large-amplitude stable spatial patterns. Although this mechanism for the development of spatially inhomogeneous patterns is well-understood, and has been applied to a broad range of specific RD systems (cf. [7]) and modeling scenarios on various spatial scales, what is less well-understood is the effect on pattern development of any time-delays in the reaction kinetics. Although there are now general results for the linear stability of spatially uniform steady-states under the effect of a time-delay (cf. [2]), which have been applied to the Gierer-Meinhardt (GM) model with saturated and time-delayed reaction kinetics in [1], the effect of time-delays in the reaction kinetics on localized RD patterns is not nearly as well understood.

Time-delays in the reaction kinetics for modeling RD patterns on a cellular spatial scale are thought to be an important biological mechanism, as there typically exists a time-delay between the initiation of protein signal transduction and the time at which genes are ultimately produced (cf. [7]). In an effort to understand the effect of such gene expression time-delays on pattern formation, various new two-component activator-inhibitor RD models with a fixed time delay in the reaction kinetics were developed based on various hypothetical sub-cellular gene expression processes in [7], [15], [16], [17] (see also the survey [18]). In these studies, pattern formation aspects of the time-delayed RD models were examined through a Turing-type linear stability around a homogeneous steady-state and from large-scale numerical computations of the PDE system on both fixed and slowly growing spatial domains. For some of these activator-inhibitor models with time-delayed kinetics, related to the classical GM model and its variants (cf. [8]), it was shown that the delay induces temporal oscillations in the spatial patterning, and that these oscillations can become very large and uncontrolled as the time-delay increases, thereby suggesting a global breakdown of a robust stable patterning mechanism.

In [6], this de-stabilizing effect of a time-delay in the reaction kinetics was analyzed in detail for a general class of GM models with a time-delay in either the inhibitor kinetics or in both the activator and inhibitor kinetics. This study of [6], and the numerical simulations in [15], leads to the question of whether a time-delay in the reaction-kinetics can ever be a stabilizing effect on pattern formation. The main new goal of this paper is to show that a time-delay in *only* the autocatalytic term of the activator kinetics actually leads to an increase in the parameter range where localized spatial patterns are linearly stable. This stabilizing effect of a time-delay in the activator kinetics will be analyzed in detail for

*Oxford Center for Industrial and Applied Mathematics (OCIAM), Oxford University, Oxford, UK

†Dept. of Mathematics, UBC, Vancouver, Canada. (corresponding author ward@math.ubc.ca)

‡Dept. of Mathematics, UBC, Vancouver, Canada.

the GM model with prototypical exponents of the nonlinearities.

The GM model [8] for the prototypical exponent set in the semi-strong interaction limit is a singularly perturbed two-component RD system with a large diffusivity ratio. For the case where only the nonlinear activator kinetics has a finite time delay T , the activator and inhibitor concentrations v and u , respectively, in a bounded domain $\Omega \in \mathbb{R}^N$ are solutions to the non-dimensional system

$$v_t = \varepsilon^2 \Delta v - v + v_T^2/u, \quad \mathbf{x} \in \Omega; \quad \tau u_t = D \Delta u - u + \varepsilon^{-N} v_T^2, \quad \mathbf{x} \in \Omega; \quad \partial_n u = \partial_n v = 0, \quad \mathbf{x} \in \partial\Omega. \quad (1.1)$$

Here $0 < \varepsilon \ll 1$, $v_T \equiv v(\mathbf{x}, t - T)$, and the reaction-time constant τ and inhibitor diffusivity D are both $\mathcal{O}(1)$ positive parameters. In the limit $\varepsilon \rightarrow 0$, it is well-known that the steady-state GM model has localized spike solutions whereby v concentrates at certain points in Ω . We will study the linear stability of these spike solutions for three different variants of this GM model with delayed activator kinetics: a one-spike solution for the 1-D shadow problem corresponding to the large inhibitor diffusivity limit $D \rightarrow \infty$, a one-spike solution in 1-D on the infinite line, and an M -spot pattern with $M \geq 2$ in a bounded 2-D domain in the weak-coupling regime $D = \mathcal{O}(-\log \varepsilon)$. The study of these three variants of the GM model will show in a rather broad sense the stabilizing effect of delayed activator kinetics on the linear stability of localized spike solutions.

In the traditional scenario where there is no activator delay, results characterizing the existence of a Hopf bifurcation threshold value of τ have been derived for the 1-D shadow problem in [22] and [10], for the 1-D infinite-line problem in [5] and [23], and for the 2-D multi-spot problem in [26]. These previous results are all based on linearizing the RD system around a localized spike (1-D) or spot (2-D) steady-state solution and then studying the spectrum of a nonlocal eigenvalue problem (NLEP) that arises from the linearized stability problem. For the two 1-D problems, these previous results with undelayed kinetics show that a one spike-solution is linearly stable only when $0 < \tau < \tau_{H0}$, and that a Hopf bifurcation occurs as τ crosses above some threshold τ_{H0} . Qualitatively similar results were found for the 2-D problem in [26], although the analysis and results in [26] were more intricate owing to the existence of two distinct modes of instability for the amplitudes of the spots, representing either in-phase (synchronous) or anti-phase (asynchronous) instabilities of the amplitudes of the spots. Overall, the qualitative mechanism for an oscillatory instability is that as τ increases, the inhibitor field can only respond relatively slowly to any local increase in the activator concentration due to the autocatalytic term. Such a slow response by the inhibitor field leads to an instability of the spike.

The goal of this paper is to show for each of these three variants of the GM model that the effect of a time-delay in the activator kinetics is *stabilizing* in the sense that there is a larger parameter range of τ , as compared with the corresponding undelayed problems, where the steady-state spike (1-D) or spot (2-D) patterns are linearly stable. In particular, for the 1-D shadow and infinite-line problems we will show, using a combined analytical and numerical study of the associated NLEP, that the Hopf bifurcation threshold for τ is a monotone increasing function of the delay T . A simple scaling law for this Hopf bifurcation threshold for the case of large delay $T \gg 1$ is derived analytically for the two 1-D problems. Similar results showing that an activator time-delay has a stabilizing effect on 2-D multi-spot patterns are obtained from a combined analytical and numerical study of the two specific NLEPs that are associated with either asynchronous or synchronous instabilities of the amplitudes of the spots.

The mathematical challenge of this study is that the NLEP under the effect of activator delay is difficult to analyze owing to the effect of the time-delay in both the local part of the operator as well as in the multiple of the nonlocal term. In the 1-D case, this NLEP has the form

$$L_\mu \Phi - \chi(\tau\lambda)\mu w^2 \frac{\int_{-\infty}^{\infty} w\Phi dy}{\int_{-\infty}^{\infty} w^2 dy} = \lambda\Phi, \quad -\infty < y < \infty; \quad \Phi \in H^1(\mathbb{R}), \quad \mu \equiv e^{-\lambda T}, \quad (1.2)$$

for some $\chi(\tau\lambda)$ that is analytic in $\text{Re}(\lambda) \geq 0$. In (1.2) the delayed local operator is defined by $L_\mu\Phi \equiv \Phi'' - \Phi + 2w\mu\Phi$, where $w = \frac{3}{2}\text{sech}^2(y/2)$. We will provide a new detailed analytical study of spectra of the delayed local eigenvalue problem $L_\mu\phi = \lambda\phi$ with $\phi \in H^1(\mathbb{R})$. By reducing this spectral problem to the study of hypergeometric functions, similar to that in [4], we derive transcendental equations characterizing all complex or real-valued spectra of L_μ . After deriving a few key properties of the NLEP (1.2), and then showing how the nonlocal term eliminates unstable spectra of L_μ , we use a simple numerical method together with an analytical scaling law to determine the boundary $\tau_H = \tau_H(T)$ in the τ versus T parameter space where (1.2) undergoes a Hopf bifurcation for both the 1-D shadow problem and 1-D infinite-line problem. Similar results for a related NLEP are derived in a 2-D context.

A key qualitative conclusion from our analysis is that a time-delay in only the activator kinetics has a stabilizing influence on the stability of localized spike solutions. This result is in marked contrast to the results found in [6] where a time-delay was assumed in both the activator and inhibitor kinetics, or only in the inhibitor kinetics. In the former case, the associated NLEP is (1.2) where $\chi(\tau\lambda)\mu$ is replaced by $\chi(\tau\lambda)\mu^2$, whereas in the latter case (1.2) holds, but with $L_\mu\Phi$ replaced with its undelayed counterpart $L\Phi \equiv \Phi'' - \Phi + 2w\Phi$. With either of these two seemingly slight modifications of the NLEP (1.2) induced by delayed inhibitor kinetics, it was shown in [6] that the Hopf bifurcation threshold τ_H is monotone decreasing in the delay T , and that, moreover, there is a finite non-zero critical value T^* of T for which a one-spike steady-state solution in 1-D is linearly unstable *for all* $\tau \geq 0$. In this sense, [6] showed that a steady-state spike solution can become highly unstable when inhibitor delay effects are included.

The outline of this paper is as follows. In §2, we describe the three variants of the GM model with activator time-delay and, for each variant, give the specific NLEP whose spectrum characterizes the linear stability of spike solutions. In §3, we derive a few explicit and rigorous results for spectral properties of the delayed local operator and for a general class of NLEPs in 1-D and in 2-D that are associated with delayed activator kinetics. In §4, we use the NLEP to calculate the Hopf bifurcation threshold for both the 1-D shadow and infinite-line problems, and we derive a scaling law for these boundaries in the large delay limit. Hopf bifurcation thresholds associated with the 2-D NLEP, corresponding to the 2-D multi-spot problem, are studied in §5 for both synchronous and asynchronous instabilities of the spot amplitudes. A brief discussion in §6 concludes the paper.

2. Formulation of the NLEP Problems. We first study the linear stability of a one-spike steady-state solution to two variants of the prototypical GM model [8] in one-space dimension when there is a time-delay in only the activator kinetics. Our first variant is the infinite-line problem where, without loss of generality, we take the inhibitor diffusivity as $D = 1$. This problem is formulated as

$$v_t = \varepsilon^2 v_{xx} - v + v_T^2/u, \quad \tau u_t = u_{xx} - u + \varepsilon^{-1} v_T^2, \quad -\infty < x < \infty, \quad t > 0, \quad (2.1)$$

where $v_T \equiv v(x, t - T)$. For $\varepsilon \rightarrow 0$ it was shown in [23] that a one-spike steady-state solution v_e, u_e to (2.1), which is centered at $x = 0$, is given by

$$v_e(x) \sim U_0 w(\varepsilon^{-1}x), \quad u_e(x) \sim U_0 e^{-|x|}, \quad U_0 = 2 \left(\int_{-\infty}^{\infty} w^2 dy \right)^{-1}, \quad (2.2)$$

where $w(y) = \frac{3}{2}\text{sech}^2(y/2)$ is the homoclinic solution on $-\infty < y < \infty$ to $w'' - w + w^2 = 0$ with $w(0) > 0, w'(0) = 0$, and $w \rightarrow 0$ as $|y| \rightarrow \infty$.

In addition, we will study the so-called limiting shadow problem for $v(x, t)$ and $u(t)$ (cf. [10]) on the interval $|x| \leq 1$, which corresponds to taking the large inhibitor diffusivity limit $D \rightarrow \infty$ in (1.1). This shadow problem is

$$v_t = \varepsilon^2 v_{xx} - v + v_T^2/u, \quad -1 < x < 1, \quad v_x(\pm 1, t) = 0; \quad \tau u_t = -u + \frac{1}{2\varepsilon} \int_{-1}^1 v_T^2 dx. \quad (2.3)$$

For $\varepsilon \rightarrow 0$, a one-spike steady-state solution v_e, u_e for (2.3) is given by (cf. [10])

$$v_e \sim u_e w(x/\varepsilon), \quad u_e \sim 2 \left(\int_{-\infty}^{\infty} w^2 dy \right)^{-1}. \quad (2.4)$$

To study the linear stability of the steady-state solution for each of these two models we linearize either (2.1) or (2.3) about the steady-state by introducing $v = v_e + e^{\lambda t} \Phi(x/\varepsilon)$, and $u = u_e + e^{\lambda t} \eta$. After a short calculation, similar to that done in [6], we obtain that $\Phi(y)$ and λ are eigenpairs of the nonlocal eigenvalue problem (NLEP)

$$L_\mu \Phi - \chi(\tau\lambda) \mu w^2 \frac{\int_{-\infty}^{\infty} w \Phi dy}{\int_{-\infty}^{\infty} w^2 dy} = \lambda \Phi, \quad -\infty < y < \infty; \quad \Phi \rightarrow 0 \quad \text{as } |y| \rightarrow \infty, \quad \mu \equiv e^{-\lambda T}, \quad (2.5a)$$

where the delayed local operator, L_μ , is defined by $L_\mu \Phi \equiv \Phi'' - \Phi + 2w\mu\Phi$. In (2.5a), the multiplier χ of the nonlocal term for either the infinite-line or shadow problems is

$$\chi(\tau\lambda) \equiv \frac{2}{1 + \tau\lambda}, \quad (\text{shadow problem}); \quad \chi(\tau\lambda) \equiv \frac{2}{\sqrt{1 + \tau\lambda}}, \quad (\text{infinite-line problem}). \quad (2.5b)$$

In (2.5b) we must specify the principal branch of $\sqrt{1 + \tau\lambda}$ (cf. [23]).

The NLEP (2.5) characterizes the linear stability of a one-spike solution on an $\mathcal{O}(1)$ time-scale to perturbations in the amplitude of the spike (cf. [23], [6]). It is readily shown that any unstable eigenvalue of (2.5), satisfying $\text{Re}(\lambda) > 0$, must be a root of $g(\lambda) = 0$, where

$$g(\lambda) \equiv \frac{1}{\mu\chi(\tau\lambda)} - \mathcal{F}_\mu(\lambda); \quad \mathcal{F}_\mu(\lambda) \equiv \frac{\int_{-\infty}^{\infty} w [(L_\mu - \lambda)^{-1} w^2] dy}{\int_{-\infty}^{\infty} w^2 dy}, \quad \mu \equiv e^{-\lambda T}. \quad (2.6)$$

2.1. The 2-D NLEP Problem. Next, we formulate the linear stability problem for an M -spot pattern, with $M \geq 2$, for the GM model (1.1) with delayed activator kinetics in a bounded 2-D domain. A localized spot pattern is one for which the steady-state solution for v concentrates at a discrete set of points $\mathbf{x}_j \in \Omega$, for $j = 1, \dots, M$, as $\varepsilon \rightarrow 0$. For the 2-D GM model with no delayed reaction kinetics, in [26] the linear stability properties of such patterns were analyzed in the weak coupling regime $D = \mathcal{O}(\nu^{-1})$ where $\nu = -1/\ln \varepsilon$. By setting $D = D_0/\nu$ in (1.1) with $N = 2$, we can readily extend the analysis of [26] to show that the linear stability of an M -spot solution with delayed activator kinetics, and with $\tau = \mathcal{O}(1)$, is characterized by the spectrum of the NLEP

$$L_\mu \Phi - \chi(\tau\lambda) \mu w^2 \frac{\int_0^\infty \rho w \Phi d\rho}{\int_0^\infty \rho w^2 d\rho} = \lambda \Phi, \quad 0 < \rho < \infty; \quad \Phi'(0) = 0, \quad \Phi \rightarrow 0 \quad \text{as } \rho \rightarrow \infty, \quad (2.7a)$$

where $L_\mu \Phi \equiv \Delta_\rho \Phi - \Phi + 2w\mu\Phi$, $\mu \equiv e^{-\lambda T}$, and $\Delta_\rho \Phi \equiv \partial_{\rho\rho} \Phi + \rho^{-1} \partial_\rho \Phi$: Here $w(\rho)$ is the positive radially symmetric ground-state solution to $\Delta_\rho w - w + w^2 = 0$ with $w(0) > 0$, $w'(0) = 0$, and $w \rightarrow 0$ as $\rho \rightarrow \infty$. In (2.7a), $\chi(\tau\lambda)$ can assume either of the two forms (cf. [26])

$$\chi(\tau\lambda) \equiv \frac{2}{1 + \beta}, \quad (\text{asynchronous mode}); \quad \chi(\tau\lambda) \equiv \frac{2}{1 + \beta} \left(\frac{1 + \beta + \tau\lambda}{1 + \tau\lambda} \right), \quad (\text{synchronous mode}), \quad (2.7b)$$

where $\beta \equiv 2\pi M D_0 / |\Omega|$ and $|\Omega|$ is the area of Ω . These two choices for χ correspond to either asynchronous (anti-phase) or synchronous (in-phase) instabilities of the amplitudes of the spots (cf. [26]). Both such modes of instability are possible when $M \geq 2$. Although there are $M - 1$ possible anti-phase modes of instability of the spot amplitudes, from the leading-order asymptotic theory of [26] leading to (2.7b) with $\chi = 2/(1 + \beta)$, these modes have a common stability threshold. With either form for χ , the discrete eigenvalues of the NLEP (2.7) are roots $g(\lambda) = 0$, where

$$g(\lambda) \equiv \frac{1}{\mu\chi(\tau\lambda)} - \mathcal{F}_\mu(\lambda); \quad \mathcal{F}_\mu(\lambda) \equiv \frac{\int_0^\infty \rho w [(L_\mu - \lambda)^{-1} w^2] d\rho}{\int_0^\infty \rho w^2 d\rho}, \quad \mu \equiv e^{-\lambda T}. \quad (2.8)$$

3. Some General Results for the Delayed Operator. For either $N = 1$ or $N = 2$, in this section we derive some properties for the general NLEP for $\Phi = \Phi(\mathbf{y})$, given by

$$L_\mu \Phi - \chi(\tau\lambda)\mu w^2 \frac{\int w \Phi}{\int w^2} = \lambda \Phi, \quad \Phi \in H^1(\mathbb{R}^N); \quad L_\mu \Phi = \Delta \Phi - \Phi + 2\mu w \Phi, \quad \mu \equiv e^{-\lambda T}, \quad (3.1)$$

where $\chi(\tau\lambda)$ is given in (2.5b) when $N = 1$ and in (2.7b) when $N = 2$. For simplicity of notation, for $N = 1$ in (3.1) we have $\Phi = \Phi(y)$, $w = w(y) = \frac{3}{2}\text{sech}^2(y/2)$ and the integration in (3.1) is over the real line. For $N = 2$, we have $\Phi = \Phi(\rho)$ and $w = w(\rho)$, with $\rho = |\mathbf{y}|$, and the integration in (3.1) is over \mathbb{R}^2 . With this notation, it readily follows that the eigenvalues λ of (3.1) are the roots of $g(\lambda) = 0$, where

$$g(\lambda) \equiv \frac{1}{\chi(\tau\lambda)\mu} - \mathcal{F}_\mu(\lambda), \quad \mathcal{F}_\mu(\lambda) \equiv \frac{\int w [(L_\mu - \lambda)^{-1} w^2]}{\int w^2}. \quad (3.2)$$

To analyze (3.2), we must first consider some properties of the delayed local eigenvalue problem, defined by

$$L_\mu \Phi = \lambda \Phi, \quad \Phi \in H^1(\mathbb{R}^N). \quad (3.3)$$

This is done in detail for $N = 1$ in §3.1 by using an analysis based on hypergeometric functions. Some partial results for the case $N = 2$ are given in §3.2.

3.1. Delayed Local Operator: One-Dimensional Case. When $N = 1$, we can derive transcendental equations for all of the eigenvalues (complex or real) of (3.3) by following the approach used in [25] for the case where μ is a fixed complex constant. For the convenience of the reader, the derivation of these equations is given in Appendix A.

As shown in (A.10) of Appendix A (see also page 1071 of [25]), we obtain that any eigenvalue λ of (3.3) when $N = 1$ must be a root of one of the transcendental equations $\mathcal{K}_l(\lambda) = 0$, for $l = 0, 1, 2, \dots$, defined by

$$\mathcal{K}_l(\lambda) \equiv 4\sqrt{1+\lambda} + 1 - \sqrt{1+48\mu} + 2l = 0, \quad l = 0, 1, 2, \dots; \quad \mu \equiv e^{-\lambda T}. \quad (3.4)$$

We first observe that the translation mode $\lambda = 0$, $\Phi = w'$, must be an eigenpair for all $T \geq 0$. This eigenvalue corresponds to setting $l = 1$ in (3.4).

Next, we characterize any non-zero real-valued eigenvalue satisfying $\lambda > -1$ that exists *for all* $T \geq 0$. It is easy to see that such eigenvalues can only occur when $l = 0$ or $l = 2$ in (3.4). In particular, for the case $l = 0$, we calculate that $\mathcal{K}_0(0) < 0$, $\mathcal{K}_0(\lambda) \rightarrow +\infty$ as $\lambda \rightarrow +\infty$, and $\mathcal{K}_0(\lambda)$ is monotone increasing on $\lambda > 0$. Consequently, (3.4) with $l = 0$ has a unique root $\lambda_0 = \lambda_0(T) > 0$ for any $T \geq 0$. We readily find from (3.4) that $\lambda_0(0) = 5/4$, $\lambda_0 \sim \log(2)/T$ for $T \gg 1$, and $\lambda_0(T)$ is monotone decreasing in T . In the left panel of Fig. 3.1 we plot $\lambda_0(T)$ versus T , as computed numerically from (3.4). The only other real non-zero eigenvalue that exists for any $T \geq 0$ is obtained from (3.4) with $l = 2$. Since $\mathcal{K}_2(-1) < 0$, $\mathcal{K}_2(0) = 2 > 0$, and $\mathcal{K}_2(\lambda)$ is monotone increasing in λ , $\mathcal{K}_2(\lambda) = 0$ has a unique root $\lambda_2(T)$ satisfying $-1 < \lambda_2(T) < 0$ for any $T \geq 0$. We readily find that $\lambda_2 \rightarrow -3/4$ as $T \rightarrow 0$ and $\lambda_2 \sim \log(3/5)/T$ for $T \gg 1$.

Next, we observe from (3.4) for $l \geq 3$ that a discrete real eigenvalue emerges from the continuous spectrum $\lambda \leq -1$ when the delay T exceeds a critical threshold $T_{\text{edge}}^l > 0$. By setting $\mathcal{K}_l(-1) = 0$ and solving for T , we identify that

$$T_{\text{edge}}^l \equiv \log\left(\frac{l^2 + l}{12}\right), \quad l = 3, 4, \dots, \quad (3.5)$$

so that $T_{\text{edge}}^{l+1} > T_{\text{edge}}^l$. Curiously, we find $T_{\text{edge}}^3 = 0$, so that a discrete real eigenvalue emerges as soon as the delay is turned on. Since for each $l \geq 3$ we have $\mathcal{K}_l(0) > 0$, $\mathcal{K}_l(\lambda)$ is monotone increasing on $-1 < \lambda < 0$, and $\mathcal{K}_l(-1) < 0$ whenever

$T > T_{\text{edge}}^l$, it follows that there is a unique root $\lambda_l(T)$ to (3.4) in $-1 < \lambda < 0$ when $T > T_{\text{edge}}^l$. A simple calculation using (3.4) shows that, for each $l \geq 3$, this eigenvalue has the following limiting asymptotics:

$$\lambda_l(T) \sim c_l/T, \quad c_l \equiv \log \left(\frac{12}{(l+3)(l+2)} \right), \quad \text{as } T \rightarrow \infty. \quad (3.6)$$

This expression shows that all of these discrete eigenvalues that bifurcate from the continuous spectrum at critical values of the delay eventually accumulate on the stable side of the origin $\lambda = 0$ as $T \rightarrow \infty$.

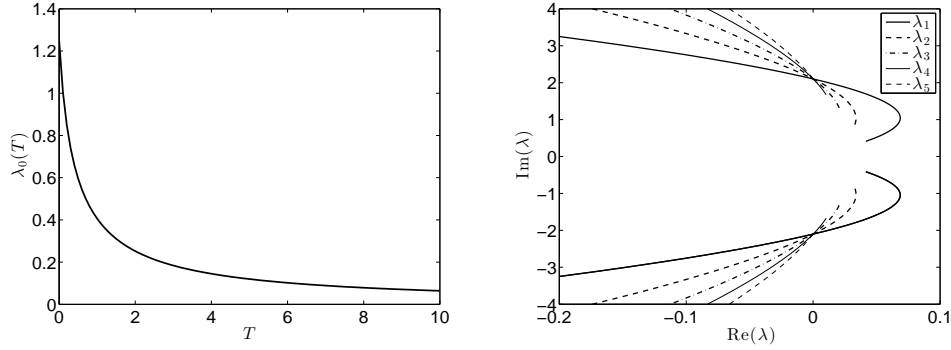


Fig. 3.1: Left panel: The positive real eigenvalue $\lambda_0(T)$ of the delayed local problem $L_\mu \Phi = \lambda \Phi$ when $N = 1$ as obtained by solving (3.4) numerically with $l = 0$. Right panel: all the paths of complex-valued spectra of L_μ in $\text{Re}(\lambda) \geq 0$ for $T_{\text{H}}^1 \leq T \leq T_{\text{H}}^5$, as computed from (3.4) for $l = 0$. Here T_{H}^j for $j \geq 1$ is the j -th value of T where L_μ has a pure imaginary eigenvalue $\lambda = i\lambda_I$ with $\lambda_I \approx 2.1015$ (see (3.10)). The path with imaginary eigenvalue when $T = T_{\text{H}}^j$ is labeled by λ_j . For even larger values of T , these paths all tend to the origin $\lambda = 0$, but in the half-space $\text{Re}(\lambda) > 0$. For each path, we also plot its continuation into $\text{Re}(\lambda) < 0$ for smaller delays.

In summary, with regards to real-valued eigenvalues of L_μ when $N = 1$, the spectral problem (3.3) has exactly three real eigenvalues that exist for any $T \geq 0$. They are $\lambda = \lambda_0(T) > 0$, $\lambda = 0$, and $\lambda = \lambda_2(T)$, where $-1 < \lambda_2(T) < 0$. In addition, real eigenvalues bifurcate from the edge $\lambda = -1$ of the continuous spectrum at the critical values T_{edge}^l for $l = 3, 4, \dots$ of the delay, as given explicitly in (3.5). For each $l \geq 3$, this additional real eigenvalue remains in $-1 < \lambda < 0$ for all $T \geq T_{\text{edge}}^l$, and it tends to the origin as $T \rightarrow \infty$ with the asymptotic rate given in (3.6).

Next, we consider complex-valued roots of (3.4). We will only characterize those complex-valued branches of roots of (3.4) as T is varied that can exist in the unstable right-half plane $\text{Re}(\lambda) \geq 0$. To do so, we first focus on determining any values of the delay T for which (3.3) has a pure imaginary eigenvalue $\lambda = i\lambda_I$ with $\lambda_I > 0$. As shown in Appendix A, (3.4) can only have a pure imaginary root $\lambda = i\lambda_I$ for the case $l = 0$. As derived in Appendix A, such a pure imaginary eigenvalue occurs at the discrete values T_{H}^n , given by

$$T = T_{\text{H}}^n \equiv \frac{(\theta_0 + 2\pi n)}{\lambda_I}, \quad n = 1, 2, 3, \dots \quad (3.7)$$

Here λ_I , which is independent of n , is given explicitly by

$$\lambda_I = \frac{1}{8} \text{Re} \left(-1 + \sqrt{1 + 48\mu} \right) \text{Im} \left(\sqrt{1 + 48\mu} \right), \quad \mu \equiv e^{-i(\theta_0 + 2\pi n)} = \cos \theta_0 - i \sin \theta_0, \quad (3.8)$$

in terms of the unique root θ_0 in $-\pi/3 \leq \theta \leq 0$ of the function $\mathcal{H}(\theta)$, defined by

$$\mathcal{H}(\theta) \equiv (24 \cos \theta - 7)^2 (12 \cos^2 \theta - 8 \cos \theta + 1) - 12 \sin^2 \theta. \quad (3.9)$$

The uniqueness of this root follows from the fact that $\mathcal{H}(0) > 0$, $\mathcal{H}(-\pi/3) < 0$, and $\mathcal{H}(\theta)$ is monotonic on $-\pi/3 < \theta < 0$.

From simple numerical computations based on this explicit characterization, we obtain that $\theta_0 \approx -0.99046$ and $\lambda_I \approx 2.1015$. The first few critical values of the delay are

$$T_H^1 \approx 2.5185, \quad T_H^2 \approx 5.5084, \quad T_H^3 \approx 8.4982, \quad T_H^4 \approx 11.488, \quad T_H^5 \approx 14.478. \quad (3.10)$$

With these explicit values for which (3.4) has a pure imaginary eigenvalue when $l = 0$, we then readily use Newton's method on (3.4) with $l = 0$ and numerically path-follow branches of spectra of L_μ for $T > T_H^n$. As shown in the right panel of Fig. 3.1 for $n = 4$, these branches lie in the unstable right-half plane $\text{Re}(\lambda) > 0$ and accumulate near $\lambda = 0$ as $T \rightarrow \infty$. By path-following these same branches on the range $0 < T < T_H^n$ these branches of spectra are in $\text{Re}(\lambda) < 0$, as expected, and were created from a singular limit process $T \rightarrow 0^+$ and $|\lambda| \gg 1$ with $\text{Re}(\lambda) < 0$. This singular behavior as $T \rightarrow 0^+$ is a well-known feature of quasipolynomials in the eigenvalue parameter that arise as the characteristic equation for traditional ODE delay equations.

Finally, we briefly discuss a general method to determine all the eigenvalues of L_μ with $N = 1$ that exist near the origin $\lambda = 0$ in the limit $T \rightarrow \infty$. This approach is based on the following result:

Lemma 3.1. *Consider the auxiliary spectral problem for $\Psi(y)$ and ξ on $-\infty < y < \infty$ given by*

$$\Psi'' - \Psi + \xi w \Psi = 0, \quad \Psi \in H^1(\mathbb{R}). \quad (3.11)$$

There is a countably infinite number of eigenvalues ξ_l for $l = 0, 1, 2, \dots$, with $\xi_l < \xi_{l+1}$ for $l \geq 0$, given explicitly by

$$\xi_0 = 1, \quad \xi_1 = 2; \quad \xi_l = \frac{(l+2)(l+3)}{6}, \quad l = 2, 3, \dots \quad (3.12)$$

The first two eigenfunctions are $\Psi_0 = w$ and $\Psi_1 = w'$.

Proof: We simply set $\lambda = 0$ and $\mu = \xi/2$ in (3.4) to obtain $5 + 2l = \sqrt{1 + 24\xi}$. Upon solving for ξ , we obtain (3.12). The first two eigenfunctions follow trivially from using $w'' - w + w^2 = 0$ and $(w')'' - w' + 2ww' = 0$. \square

We now illustrate the use of this lemma by seeking all eigenvalues of L_μ near $\lambda = 0$ when $T \gg 1$. We let $\lambda \sim c/T$ for $T \gg 1$ and from (3.3) obtain that

$$\Phi'' - \Phi + 2[e^{-c} + \mathcal{O}(T^{-1})]w\Phi = \mathcal{O}(T^{-1})\Phi.$$

To leading order we put $\Phi = \Psi + \mathcal{O}(T^{-1})$ so that Ψ is an eigenfunction of (3.11) with eigenvalue $\xi \equiv 2e^{-c}$. These eigenvalues are given in (3.12). If we set $\xi_0 = 1$, we have $1 = 2e^{-c}$, so that $c = \log(2) + 2n\pi i$ for $n = 0, \pm 1, \pm 2, \dots$. This gives $\lambda \sim [\log(2) + 2n\pi i]/T$ for $T \gg 1$. Setting $n = 0$, we obtain the asymptotics of the positive real eigenvalue $\lambda_0(T) \sim \log(2)/T$, derived earlier. In addition, the choices $n = \pm 1, \pm 2, \dots$ correspond to the limiting behavior as $T \rightarrow \infty$ of the paths of complex-valued eigenvalues in $\text{Re}\lambda > 0$ (see the right panel of Fig. 3.1). In contrast, if we use ξ_l in (3.12) with $l \geq 2$, we obtain $e^{-c} = \xi_l/2$ for $l \geq 2$. This yields the large T behavior for the negative real eigenvalues $\lambda_l(T)$ for $l \geq 2$, as given in (3.6).

3.2. Delayed Local Operator: Two-Dimensional Case. When $N = 2$, the explicit expression (3.4) no longer holds, and so only we must proceed indirectly and through numerical computations. For positive real eigenvalues we can still claim the following:

Lemma 3.2. *For each $T \geq 0$, there exists a unique eigenvalue real positive eigenvalue $\lambda = \lambda_0(T)$ to (3.3).*

Proof: For each $\mu \in (\frac{1}{2}, 1)$, it is easy to see that there exists a unique principal eigenvalue, called $\lambda(\mu)$, to (3.3), with positive principal eigenfunction. In fact, it admits the variational characterization

$$-\lambda(\mu) = \inf_{\phi \in H^1(\mathbb{R}^2), \phi \neq 0} \frac{\int (|\nabla \phi|^2 + \phi^2) - 2\mu w \phi^2}{\int \phi^2}. \quad (3.13)$$

We only consider the range $\mu > 1/2$, since if $\mu < 1/2$, i.e. $2\mu < 1$, it holds from Lemma 5.1 (part 2) of [25]

$$\int (|\nabla\phi|^2 + \phi^2) - w\phi^2 \geq 0, \quad (3.14)$$

where the equality holds iff $\phi = Cw$. Hence for $\mu \leq 1/2$, $\lambda(\mu) \leq 0$ and if $\mu = 1/2$, then $\lambda(1/2) = 0$ is the principal eigenvalue with eigenfunction w . For $\mu > 1/2$, we have $\lambda(\mu) > 0$, as can be verified by using the trial function $\phi = w$ in (3.13), which yields

$$-\lambda(\mu) \leq \frac{\int (|\nabla w|^2 + w^2) - 2\mu w^3}{\int w^2} = (1 - 2\mu) \frac{\int w^3}{\int w^2}, \quad (3.15)$$

This implies $\lambda(\mu) > 0$ when $\mu > 1/2$. Next, for $\mu = 1$ we recall that L_1 admits only one positive eigenvalue ν_0 , and that the second eigenvalue is zero. By a min-max variational characterization of eigenvalues based on (3.13), it follows that the eigenvalues of L_μ are monotone decreasing in μ . Thus for $\mu < 1$, the second eigenvalue L_μ , is strictly less than the second eigenvalue of L_1 , which is 0. Therefore, the only positive eigenvalue is the first eigenvalue and hence it is principal, which must be simple by definition. By uniqueness, $\lambda(\mu)$ is a smooth function of μ . Then, recalling $\mu = e^{-\lambda T}$, the problem (3.3) can be rewritten as the transcendental equation

$$\lambda(\mu) = -\frac{\log \mu}{T}. \quad (3.16)$$

Note that $\lambda(1/2) = 0$ while $\lambda(1) = \nu_0$, and $\lambda(\mu)$ is an increasing of μ . On the other hand, the right-hand side of (3.16) is a decreasing function of μ . Hence there exists a unique μ satisfying (3.16). This implies that there exists a unique positive real eigenvalue $\lambda = \lambda_0$ to (3.3). \square

We now relabel this unique positive eigenvalue of (3.3) as $\lambda_0(T)$. Next, for $N = 2$, we determine approximations to $\lambda_0(T)$ that are valid when either $T \ll 1$ or $T \gg 1$. We first determine an approximation valid for small delay. When $T = 0$, we know that $L_1\Psi = \nu\Psi$ with $\Psi \rightarrow 0$ as $\rho \rightarrow \infty$ has a unique positive eigenvalue ν_0 with eigenfunction $\Psi_0 > 0$ (cf. [26]). To determine an approximation for $T \ll 1$ we perform a standard perturbation analysis of a simple eigenvalue. We write $\lambda_0 = \nu_0 + T\nu_1 + \dots$ and $\phi_0 = \Psi + T\phi_1 + \dots$. Upon substituting these expansions into $L_\mu\phi = \lambda_0\phi$, and equating the $\mathcal{O}(T)$ terms, we obtain that

$$(L_1 - \nu_0)\phi \equiv \Delta_\rho\phi - \phi_1 + 2w\phi_1 - \nu_0\phi_1 = \nu_1\Psi_0 + 2\nu_0w\Psi_0.$$

Since $(L_1 - \nu_0)\Psi_0 = 0$, and L_1 is self-adjoint, the solvability condition for this problem is that the right-hand side of this expression is orthogonal to Ψ_0 . This determines ν_1 .

To determine an approximation for large delay we use the scaling law ansatz $\lambda_0 \sim \lambda_c/T$ for $T \gg 1$, which yields that $\Delta_\rho\phi - \phi + 2[e^{-\lambda_c} + \dots]w\phi = \mathcal{O}(T^{-1})$. Therefore, $\phi = w + \mathcal{O}(T^{-1})$, and upon using $\Delta_\rho w - w = -w^2$, we obtain that this equation holds when $w^2(2e^{-\lambda_c} - 1) = 0$. This yields that $\lambda_c = \log 2$.

In this way, we conclude that $\lambda_0(T)$ has the following limiting asymptotics for small and large delay:

$$\lambda_0(T) \sim \nu_0 - 2\nu_0T \frac{\int_0^\infty \rho w \Psi_0^2 d\rho}{\int_0^\infty \rho \Psi_0^2 d\rho} + \dots, \quad \text{as } T \rightarrow 0; \quad \lambda_0(T) \sim \log 2/T + \dots, \quad \text{as } T \rightarrow \infty. \quad (3.17)$$

In the left panel of Fig. 3.2 we show numerical results of a Newton iteration scheme applied to $L_\mu\Phi = \lambda\Phi$ to compute $\lambda_0(T)$ for any $T > 0$ when $N = 2$. The limiting asymptotics (3.17) are found to compare favorably with these results.

Next, we study complex eigenvalues of (3.3). We first observe that if Φ, λ is an eigenpair of (3.3) then so is $\bar{\Phi}$ and $\bar{\lambda}$. We first seek a necessary condition for which $\lambda = i\lambda_I$ with $\lambda_I > 0$ is an eigenvalue of (3.3). We write $\Phi = \Phi_R + i\Phi_I$ and $\mu = e^{-i\lambda_I T} = \mu_R + i\mu_I$ in (3.3), and after separating into real and imaginary parts we get

$$\Delta\Phi_R - \Phi_R + 2w\mu_R\Phi_R - 2w\mu_I\Phi_I = -\lambda_I\Phi_I, \quad \Delta\Phi_I - \Phi_I + 2w\mu_R\Phi_I + 2w\mu_I\Phi_R = \lambda_I\Phi_R. \quad (3.18)$$

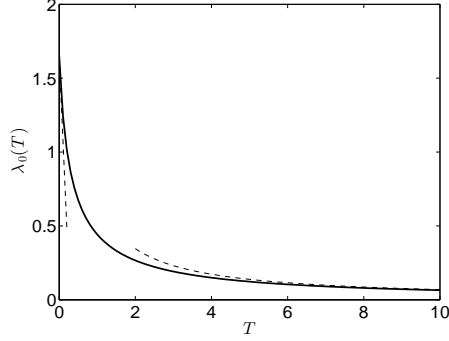


Fig. 3.2: Left panel: the positive real eigenvalue $\lambda_0(T)$ of $L_\mu\Phi = \lambda\Phi$ when $N = 2$ (solid curve), as computed numerically from a BVP solver. The asymptotic results (3.17) for small and large delay are the dashed curves.

Upon multiplying the first equation by Φ_I and the second by Φ_R , we subtract the resulting expressions and use Green's identity to obtain

$$2\mu_I \int (\Phi_I^2 + \Phi_R^2) w = \lambda_I \int (\Phi_I^2 + \Phi_R^2). \quad (3.19)$$

Since $\lambda_I > 0$, this shows that $\mu_I = -\sin(\lambda_I T) < 0$. Next, we multiply the first equation in (3.18) by Φ_R and the second by Φ_I , and add the resulting equations. After using $\nabla \cdot (\Phi_R \nabla \Phi_R) = |\nabla \Phi_R|^2 + \Phi_R \Delta \Phi_R$. This readily yields

$$2\mu_R \int (\Phi_I^2 + \Phi_R^2) w = \int (|\nabla \Phi_R|^2 + |\nabla \Phi_I|^2 + \Phi_R^2 + \Phi_I^2), \quad (3.20)$$

so that $\mu_R = \cos(\lambda_I T) > 0$ at any HB point. In summary, we have shown that at any HB point with $\lambda_I > 0$ we must have $\cos(\lambda_I T) > 0$ and $\sin(\lambda_I T) < 0$.

The next result establishes the existence of a HB point for L_μ when $N = 2$.

Lemma 3.3. *The delayed local eigenvalue problem (3.3) in 2-D has a HB point.*

Proof: Let $w(\rho)$ be the ground-state solution to $\Delta_\rho w - w + w^2 = 0$ and define $\theta \equiv \lambda_I T$. We now show that there is a value θ_0 of θ for which

$$\Delta_\rho \Phi - \Phi + 2we^{-i\theta} \Phi = i\lambda_I \Phi, \quad \Phi \in H^1(\mathbb{R}^2), \quad (3.21)$$

has a solution $\lambda_I > 0$. In fact, we consider the following eigenvalue problem

$$\Delta_\rho \Phi - \Phi + 2we^{-i\theta} \Phi = \lambda \Phi, \quad \Phi \in H^1(\mathbb{R}^2), \quad (3.22)$$

where we vary $\theta \in (-\frac{\pi}{3}, 0)$. When $\theta = 0$, $e^{-i\theta} = 1$, it is known that (3.22) has a unique positive eigenvalue. On the other hand, when $\theta = -\pi/3$, so that $e^{-i\theta} = \frac{1}{2} + i\frac{\sqrt{3}}{2}$, we claim that all eigenvalues of (3.22) must lie on the left-hand side of the complex λ plane. To see this, we multiply (3.22) by the conjugate of Φ and integrate to obtain the identity

$$-\int (|\nabla \Phi|^2 + |\Phi|^2 - 2\cos(\theta)w|\Phi|^2) = \lambda_R \int |\Phi|^2, \quad (3.23)$$

and

$$-2\sin(\theta) \int (w|\Phi|^2) = \lambda_I \int |\Phi|^2. \quad (3.24)$$

Upon setting $\cos(\theta) = 1/2$, we observe from (3.23) and (3.14) that $-\lambda_R \geq 0$, so that $\lambda_R \leq 0$. If $\lambda_R = 0$, we must have $\Phi = cw$ for some constant c . Substituting into the equation, we see that this is impossible. By the continuity argument (see [3]), as θ varies from 0 to $-\frac{\pi}{3}$, the eigenvalue must cross the imaginary axis at some $\theta_0 \in (-\frac{\pi}{3}, 0)$. From (3.23) and the fact that $\sin(\theta) \neq 0$ in this open interval, we have that $\lambda \neq 0$. Therefore the crossing point must be a Hopf bifurcation point. From (3.24) we see that $\lambda_I > 0$. Since $\theta_0 \in (-\frac{\pi}{3}, 0)$, $\cos(\theta_0) > 0$ and $\sin(\theta_0) < 0$, the HB values of T are $T_H^n \equiv (\theta_0 + 2\pi n) / \lambda_I$ for $n = 1, 2, 3, \dots$ \square

From simple numerical computations of a matrix eigenvalue problem obtained from a finite difference approximation of (3.21), we calculate that $\theta_0 \approx -0.9303$ and $\lambda_I \approx 2.691$. The first few critical values of the delay are then

$$T_H^1 \approx 1.989, \quad T_H^2 \approx 4.324, \quad T_H^3 \approx 6.659, \quad T_H^4 \approx 8.995, \quad T_H^5 \approx 11.33. \quad (3.25)$$

Paths in the complex plane for $T > T_H^j$ are then similar to those shown in the right panel of Fig. 3.1 for the case $N = 1$.

3.3. A Monotonicity Property for $\mathcal{F}_\mu(\lambda)$. Next, we show for either $N = 1$ or $N = 2$ that $\mathcal{F}_\mu(\lambda)$, as defined in (3.2), is monotone increasing in $\lambda > 0$ real with $\lambda \neq \lambda_0(T)$, where $\lambda_0(T) > 0$ is the unique real positive eigenvalue of $L_\mu \Phi$.

We first compute that

$$L_\mu w = (2\mu - 1)w^2, \quad (L_\mu - \lambda)^{-1}(w^2) = \frac{1}{2\mu - 1}(L_\mu - \lambda)^{-1}(L_\mu w) = \frac{w}{2\mu - 1} + \frac{\lambda}{2\mu - 1}(L_\mu - \lambda)^{-1}(w). \quad (3.26)$$

Hence (3.2) becomes

$$g(\lambda) = \frac{1}{\chi(\tau\lambda)\mu} - \mathcal{F}_\mu(\lambda), \quad \mathcal{F}_\mu(\lambda) \equiv \frac{1}{2\mu - 1} + \frac{\lambda}{2\mu - 1}P(\lambda), \quad \text{where} \quad P(\lambda) \equiv \frac{\int w(L_\mu - \lambda)^{-1}w}{\int w^2}. \quad (3.27)$$

Therefore, upon setting $g(\lambda) = 0$, we conclude that λ must satisfy

$$\frac{1}{\chi(\tau\lambda)\mu} = \mathcal{F}_\mu(\lambda) = \frac{1}{2\mu - 1} + \frac{\lambda}{2\mu - 1}P(\lambda), \quad (3.28)$$

where $P(\lambda)$ is defined in (3.27). We now claim that $P(\lambda)$, and hence $\mathcal{F}_\mu(\lambda)$ is monotone increasing.

Lemma 3.4. *For $\lambda > 0$ real and $\lambda \neq \lambda_0(T)$, we have $P'(\lambda) > 0$.*

Proof: We define $\psi \equiv (L_\mu - \lambda)^{-1}w$, so that ψ solves

$$\Delta\psi - \psi + 2e^{-\lambda T}w\psi = \lambda\psi + w. \quad (3.29)$$

Upon differentiating this equation with respect to λ we obtain

$$\Delta\psi' - \psi' + 2e^{-\lambda T}w\psi' - \lambda\psi' = 2Te^{-\lambda T}w\psi + \psi. \quad (3.30)$$

Hence, upon using (3.27) for $P(\lambda)$, and integrating by parts, we obtain that

$$\begin{aligned} P'(\lambda) &= \frac{\int w\psi'}{\int w^2} = \frac{\int w(L_\mu - \lambda)^{-1}(2Te^{-\lambda T}w\psi + \psi)}{\int w^2} \\ &= 2Te^{-\lambda T} \frac{\int w(L_\mu - \lambda)^{-1}(w\psi)}{\int w^2} + \frac{\int w(L_\mu - \lambda)^{-1}\psi}{\int w^2}, \\ &= 2Te^{-\lambda T} \frac{\int ((L_\mu - \lambda)^{-1}w)(w\psi)}{\int w^2} + \frac{\int w(L_\mu - \lambda)^{-2}w}{\int w^2}, \\ &= 2Te^{-\lambda T} \frac{\int w\psi^2}{\int w^2} + \frac{\int w(L_\mu - \lambda)^{-2}w}{\int w^2} = 2Te^{-\lambda T} \frac{\int w\psi^2}{\int w^2} + \frac{\int [(L_\mu - \lambda)^{-1}w]^2}{\int w^2} > 0, \end{aligned}$$

which proves the claim. \square

As a remark, by using $L_1^{-1}w = w + \rho w'/2$ for $N = 2$ and $L_1^{-1}w = w + yw'/2$ for $N = 1$, we can calculate that

$$P(\lambda) > P(0) = \frac{\int w L_1^{-1} w}{\int w^2} = \frac{4 - N}{4}.$$

As a numerical confirmation of this key monotonicity result for \mathcal{F}_μ , for both $N = 1$ and $N = 2$ in Fig. 3.3 we plot $\mathcal{F}_\mu(\lambda)$, defined in (3.2), on the interval $0 < \lambda < \lambda_0(T)$ of the real λ -axis for three values of the delay T . This confirms that $\mathcal{F}_\mu(\lambda)$ is monotone increasing on this interval with $\mathcal{F}_\mu(\lambda) \rightarrow +\infty$ as $\lambda \rightarrow \lambda_0(T)$ from below. Using $L_1^{-1}w^2 = w$, it also follows that $\mathcal{F}_\mu(0) = 1$ for all $T \geq 0$. We remark that this monotonicity property is qualitatively similar to that for the undelayed operator L_1 (see [22] and [23]).

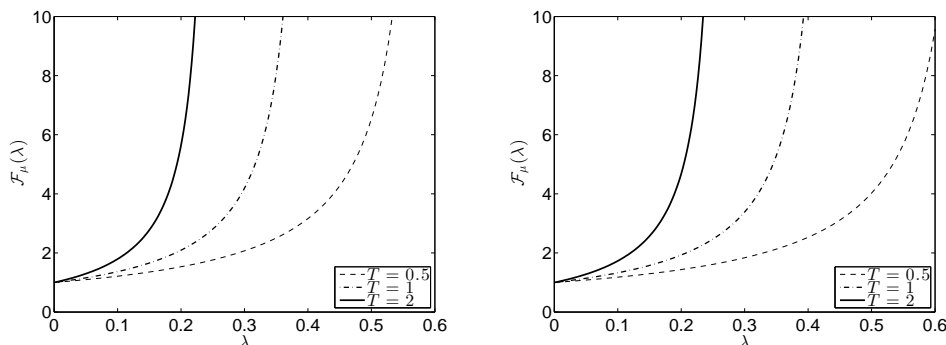


Fig. 3.3: Plot of the numerically computed function $\mathcal{F}_\mu(\lambda)$, defined in (3.2), when $N = 1$ (left panel) and when $N = 2$ (right panel) on the positive real axis for $0 < \lambda < \lambda_0(T)$ for three values of the delay T as indicated in the figure. We confirm that $\mathcal{F}_\mu(\lambda)$ is monotone increasing on $0 < \lambda < \lambda_0(T)$, with $\mathcal{F}_\mu(\lambda) \rightarrow +\infty$ as $\lambda \rightarrow \lambda_0(T)$ from below.

This monotonicity result yields two key qualitative results for the roots of (3.28), which follow immediately from the facts that $\mathcal{F}_\mu(0) = 1$, $\mathcal{F}_\mu(\lambda)$ is monotone increasing on $0 < \lambda < \lambda_0(T)$ and $\mathcal{F}_\mu(\lambda) \rightarrow \infty$ as $\lambda \rightarrow \lambda_0(T)$ from below.

Theorem 3.1. *Consider the NLEP (3.1), for which the eigenvalues are roots of (3.28). (I) Suppose that $\chi(0) < 1$. Then, the NLEP has a positive real eigenvalue on $0 < \lambda < \lambda_0(T)$ for any $T \geq 0$ and $\tau \geq 0$. (II) Fix $T \geq 0$, and suppose $\chi(0) > 1$, where $\chi(\tau\lambda)$ is given in (2.5b) and (2.7b). Then, there are at least two roots to (3.28), and hence at least two positive real eigenvalues for the NLEP (3.1), when $\tau \gg 1$.*

3.4. Continuous dependence on T . We write (3.1) in the following form:

$$\mathcal{L}_\lambda \Phi := L_\mu \Phi - \chi(\tau\lambda) \mu w^2 \frac{\int w \Phi}{\int w^2} = \lambda \Phi. \quad (3.31)$$

We claim that branches of eigenvalues of this NLEP are continuous in $T \geq 0$ on $\mathcal{S} \equiv \{\lambda \mid \text{Re}(\lambda) > -1, \chi(\tau\lambda) \text{ is analytic}\}$. We will only work in the class of radially symmetric functions. We first look at Fredholm properties. Since the map $\Phi \rightarrow \mu w \Phi - \chi(\tau\lambda) w^2$ is relatively compact as a map of H^2 to L^2 , we see that the operator $L_\mu - \lambda$ is Fredholm of index zero. Next we note that, if λ_0 is an eigenvalue of $\mathcal{L}_\lambda \Phi = \lambda \Phi$ then its geometric multiplicity on L_r^2 , where L_r is the operator L_μ restricted to the radial class, is 1 unless $\lambda = \lambda_0$. To see this, note that if we have two linearly independent eigenfunctions, a possible combination will make $\int w \phi = 0$, and hence we obtain that λ satisfies the local eigenvalue problem (3.3), which is impossible. The analyticity of our operator in λ on the set \mathcal{S} , which can be seen from the definitions, the Fredholm property and Theorem 3.6 of Gokhberg and Krein (cf. [9]) implies that all eigenvalues of (3.31) are isolated. Finally, we show that the algebraic multiplicity is also one. This follows from Dancer's argument (see page 248 of [3]).

In conclusion, we have shown that for each fixed T , the eigenvalues of (3.31) are isolated with geometric and algebraic multiplicity one. Applying the classical theory of Kato [13], we conclude the eigenvalues vary continuously in T .

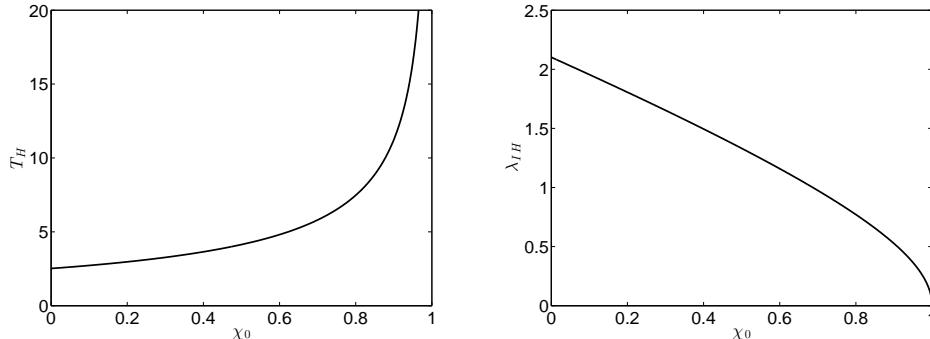


Fig. 3.4: HB threshold for (3.32) versus the constant multiplier χ_0 of the nonlocal term in (3.32). Left panel: The minimum value T_H of T versus χ_0 where a HB occurs. Right panel: The HB frequency λ_{IH} versus χ_0 . A HB occurs only on $0 \leq \chi_0 < 1$ with $\lambda_{IH} \rightarrow 0^+$ and $T_H \rightarrow +\infty$ as $\chi_0 \rightarrow 1^-$. For $\chi_0 > 1$ the NLEP (3.32) does not have any HB as T is increased.

To illustrate the use of this result, we let $N = 1$ and study numerically how the unstable complex conjugate eigenvalues for L_μ are pushed into the stable left half-plane $\text{Re}(\lambda) < 0$ for the following NLEP with a constant multiplier $\chi_0 > 0$:

$$L_\mu \Phi - \chi_0 \mu w^2 \frac{\int w \Phi}{\int w^2} = \lambda \Phi, \quad \Phi \in H^1(\mathbb{R}^1); \quad L_\mu \Phi = \Delta \Phi - \Phi + 2\mu w \Phi, \quad \mu \equiv e^{-\lambda T}. \quad (3.32)$$

As a starting point, we let $\chi_0 = 0$ and choose the minimum value T_H^1 of the delay for which L_μ has a pure imaginary eigenvalue λ_{IH} , and we then numerically track this HB point as χ_0 is increased. With this homotopy, the HB threshold value of T and frequency as a function of χ_0 are shown in the left and right panels of Fig. 3.4. From this figure, we observe that a HB occurs only when $0 \leq \chi_0 < 1$, and that $\lambda_{IH} \rightarrow 0^+$ and $T_H \rightarrow +\infty$ as $\chi_0 \rightarrow 1^-$. For $\chi_0 > 1$ the NLEP (3.32) does not undergo any HB as T is increased. Since when $T = 0$ we have $\text{Re}(\lambda) \leq 0$, with equality holding iff $\Phi = w'$ (cf. [24]), and that unstable eigenvalues can only enter $\text{Re}(\lambda) > 0$ through a HB, we conclude, by continuity in T , that $\text{Re}(\lambda) \leq 0$ for any $T > 0$ whenever $\chi_0 > 1$.

We remark that an extension of this result to $N = 2$ is used in §5.2 to characterize HB points for the NLEP (2.7) with the constant multiplier $\chi = 2/(1 + \beta)$, which applies to asynchronous instabilities of multi-spot patterns in 2-D.

4. The 1-D Problems: NLEP Computations and a Scaling Law. In this section, we consider the NLEP (2.5) for the 1-D case. From this spectral problem, we numerically determine the threshold conditions for a Hopf Bifurcation (HB) for both the infinite-line (2.1) and the shadow (2.3) problems. We also derive a scaling law for the HB thresholds in the limit of large delay T . We first note that when $\tau = 0$ in (2.5), we have $\chi(\tau\lambda) = 2$, and so by the result in §3.4 (see Fig. 3.4), we have $\text{Re}(\lambda) \leq 0$ for all $T \geq 0$. Fixing T , we have from Theorem 3.1 that there are at least two positive real eigenvalues when τ is large enough. By continuity in τ , there must be a HB at some $\tau = \tau_H > 0$ depending on T .

To determine the threshold conditions for such a HB, we set $\text{Re}(g(i\lambda_{IH})) = 0$ and $\text{Im}(g(i\lambda_{IH})) = 0$ in (2.6), where $\lambda_{IH} > 0$. This yields a 2×2 nonlinear system for the HB values τ_H and λ_{IH} at a particular value of the delay $T \geq 0$. By using Newton's method on this system, together with a numerical computation of $(L_\mu - i\lambda_{IH})^{-1}w^2$, in the left panel of Fig. 4.1 we plot the numerically computed HB boundary τ_H versus T for the shadow problem (2.3). Our numerical results show that the spike solution is linearly stable for $\tau < \tau_H$. The corresponding HB frequency λ_{IH} is plotted versus T in the middle panel of Fig. 4.1. In the right panel of Fig. 4.1 we show that τ_H/T and $\lambda_{IH}T$ both tend to finite non-zero limiting

values as $T \rightarrow \infty$. As shown in Fig. 4.2, we obtain qualitatively similar results for a HB for the infinite-line problem (2.1). Our key conclusion that τ_H is monotone increasing in T shows that a time-delay in only the activator kinetics has a stabilizing effect on a spike solution for (2.3) and (2.1).

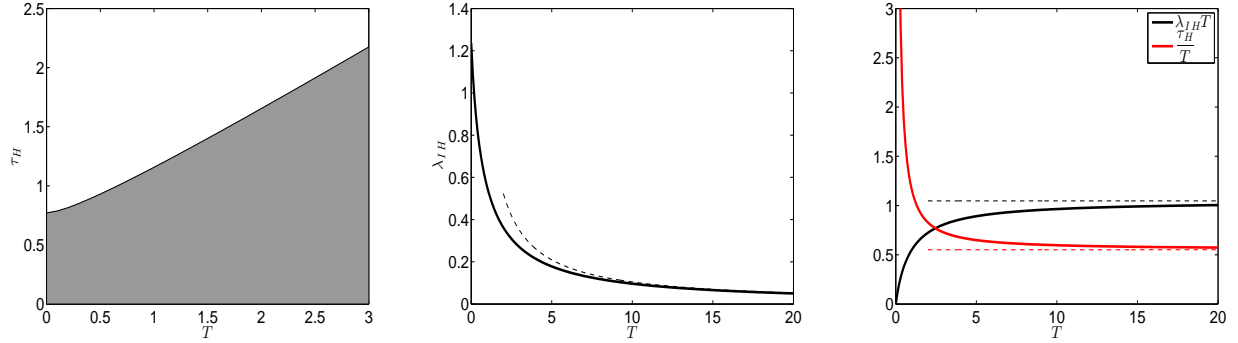


Fig. 4.1: HB threshold τ_H (left panel) and frequency λ_{IH} (solid curve in middle panel) versus T , as computed from (2.6) for the shadow problem (2.3). For $\tau < \tau_H$ (shaded region), the spike solution is linearly stable. The dashed curve in the middle panel is the large-delay asymptotic result for λ_{IH} given in (4.4). Right panel: plot of τ_H/T (monotone decreasing solid curve) and $\lambda_{IH}T$ (monotone increasing solid curve), as computed from (2.6). The asymptotes (dashed lines) are the theoretically predicted limiting values $\lim_{T \rightarrow \infty} \tau_H/T \approx \sqrt{3}/\pi$ and $\lim_{T \rightarrow \infty} \lambda_{IH}T \approx \pi/3$, as obtained from (4.4).

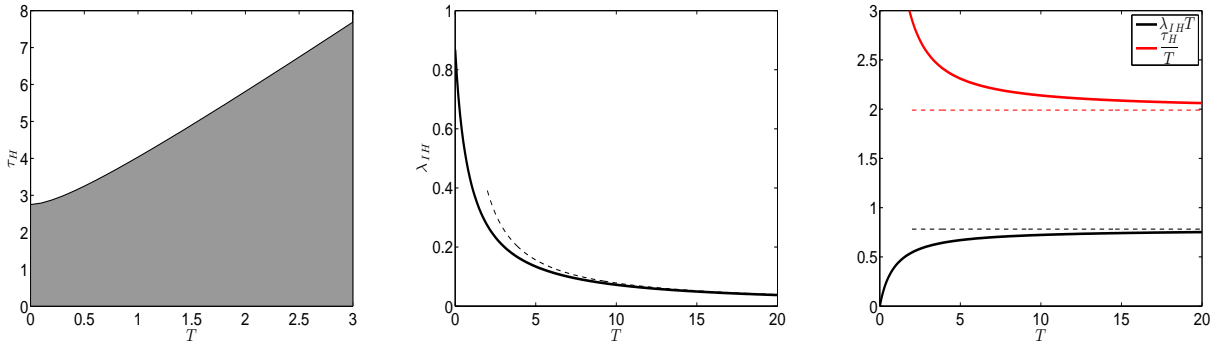


Fig. 4.2: HB values for the infinite-line problem (2.1), with the same caption as in Fig. 4.1. In the middle panel, the large-delay asymptotic result (dashed curve) is $\lambda_{IH} \sim c_0/T$ with $c_0 \approx 0.782$. In the right panel the theoretically predicted horizontal asymptotes are $\lim_{T \rightarrow \infty} \tau_H/T \approx 1.99$ and $\lim_{T \rightarrow \infty} \lambda_{IH}T \approx 0.782$, as obtained from (4.8).

The numerical results shown in Fig. 4.1 and Fig. 4.2 show that the HB threshold and frequency satisfy $\tau_H \rightarrow \infty$ and $\lambda_{IH} \rightarrow 0$ as $T \rightarrow \infty$, respectively, with τ_H/T and $\lambda_{IH}T$ both tending to finite non-zero limiting values as $T \rightarrow \infty$.

We now characterize this large delay limiting behavior analytically. Our explicit results, described below, are shown by the dashed lines in the middle and right panels of Fig. 4.1 and Fig. 4.2. For $T \rightarrow \infty$, we pose $\tau_H \sim \tau_0 T$ and $\lambda \sim ic_0/T$ for some $c_0 > 0$ and $\tau_0 > 0$ to be found. With this scaling law, (2.5a) reduces to leading-order to

$$\Phi'' - \Phi + 2w [e^{-ic_0} + \dots] \Phi - [\chi_0 e^{-ic_0} + \dots] w^2 \frac{\int_{-\infty}^{\infty} w \Phi dy}{\int_{-\infty}^{\infty} w^2 dy} = \left[\frac{ic_0}{T} + \dots \right] \Phi, \quad (4.1)$$

where $\chi_0 \equiv \chi(ic_0\tau_0)$. Since $w'' - w + w^2 = 0$, (4.1) yields that $\Phi \sim w + \mathcal{O}(T^{-1})$, provided that c_0 and τ_0 are roots to

$$e^{ic_0} = 2 - \chi_0. \quad (4.2)$$

For the shadow problem, where from (2.5b) we have $\chi = 2/(1 + \tau\lambda)$, the complex-valued equation (4.2) becomes

$$e^{ic_0} = \frac{2ic_0\tau_0}{1 + ic_0\tau_0}. \quad (4.3)$$

By setting the modulus of the right-hand side of (4.3) to unity, and defining $\xi \equiv c_0\tau_0$, we get $2\xi = \sqrt{1 + \xi^2}$, so that $c_0\tau_0 = 1/\sqrt{3}$. Then, (4.3) yields $e^{ic_0} = e^{i\pi/3}$, which has $c_0 = \pi/3$ as its minimal root. In this way, the scaling law for a HB for the shadow problem (2.3) is

$$\tau_H \sim \frac{\sqrt{3}}{\pi}T; \quad \lambda = i\lambda_{IH}, \quad \lambda_{IH} \sim \frac{\pi}{3T}, \quad \text{as } T \rightarrow \infty. \quad (4.4)$$

The asymptotics for λ_{IH} , given by the dashed curve in the middle panel of Fig. 4.1, agree well with the numerical results. In addition, the theoretically predicted horizontal asymptotes $\lim_{T \rightarrow \infty} \tau_H/T = \tau_0 \approx 0.551$ and $\lim_{T \rightarrow \infty} \lambda_{IH}T = c_0 \approx 1.047$, shown in the right panel of Fig. 4.1, agree well with the numerically computed results from (2.6).

A similar analysis can be done for the infinite-line problem where, from (2.5b), $\chi = 2/\sqrt{1 + \tau\lambda}$. Then, (4.2) becomes

$$e^{ic_0} = \frac{2[\sqrt{1 + i\tau_0 c_0} - 1]}{\sqrt{1 + i\tau_0 c_0}}. \quad (4.5)$$

By setting the modulus of the right-hand side of (4.5) to unity, we get that $2|z - 1| = |z|$, where $z \equiv \sqrt{1 + i\xi}$ and $\xi \equiv c_0\tau_0$. Upon separating z into real and imaginary parts, as $z = z_R + iz_I$, we get

$$3(z_R^2 + z_I^2) = 8z_R - 4, \quad \text{where} \quad z_R = \sqrt{\frac{\alpha + 1}{2}}, \quad z_I = \sqrt{\frac{\alpha - 1}{2}}, \quad \alpha \equiv \sqrt{1 + \xi^2}, \quad (4.6)$$

which can be combined to obtain $3\alpha = 4\sqrt{2(1 + \alpha)} - 4$. This yields that $\alpha = 4(1 + \sqrt{10})/9$, and consequently

$$\xi = c_0\tau_0 = \lim_{T \rightarrow \infty} \lambda_{IH}\tau_H = \frac{\sqrt{95 + 32\sqrt{10}}}{9} \approx 1.5563. \quad (4.7)$$

With $c_0\tau_0$ known, we take the imaginary part of (4.5) to obtain that $\sin(c_0) = 2z_I/(z_R^2 + z_I^2)$. From the expressions for z_R and z_I in (4.6), we obtain c_0 and τ_0 in terms of $\alpha = 4(1 + \sqrt{10})/9$ as

$$c_0 = \sin^{-1} \left(\frac{\sqrt{2}}{\alpha} \sqrt{\alpha - 1} \right) \approx 0.782106, \quad \tau_0 = \frac{\sqrt{95 + 32\sqrt{10}}}{9c_0} \approx 1.9899. \quad (4.8)$$

With these values of c_0 and τ_0 , the scaling law for a HB for the infinite-line problem (2.1) is $\tau_H \sim \tau_0 T$ and $\lambda = i\lambda_{IH}$ with $\lambda_{IH} \sim c_0/T$ as $T \rightarrow \infty$. The asymptotics $\lambda_{IH} \sim c_0/T$ is shown by the dashed curve in the middle panel of Fig. 4.2. The theoretically-predicted limiting values $\lim_{T \rightarrow \infty} \tau_H/T = \tau_0 \approx 1.99$ and $\lim_{T \rightarrow \infty} \lambda_{IH}T = c_0 \approx 0.782$, given by the horizontal asymptotes in the right panel of Fig. 4.2, agree well with the numerically computed results from (2.6).

4.1. Numerical Validation of the Theory. In order to readily compare our theoretical results for the HB threshold with full numerical results from the delayed RD system we need to extend our theory to the case of a finite 1-D domain $|x| \leq L$ so as to be more readily able to compute solutions to the full PDE system. As such, we consider a one-spike solution centered at $x = 0$ for the finite-domain problem

$$v_t = \varepsilon^2 v_{xx} - v + v_T^2/u, \quad \tau u_t = u_{xx} - u + \varepsilon^{-1} v_T^2, \quad |x| \leq L, \quad t > 0, \quad (4.9)$$

where $v_x = u_x = 0$ at $x = \pm L$. By first constructing a one-spike solution and then analyzing the linear stability problem, a simple calculation, similar to that in [6] and [23], shows that the linear stability problem reduces to determining the roots of (2.6), where $\chi(\tau\lambda)$ is now defined in terms of the principal branch of $\sqrt{1 + \tau\lambda}$ by

$$\chi(\tau\lambda) = \frac{2}{\sqrt{1 + \tau\lambda}} \left(\frac{\tanh(L)}{\tanh(L\sqrt{1 + \tau\lambda})} \right). \quad (4.10)$$

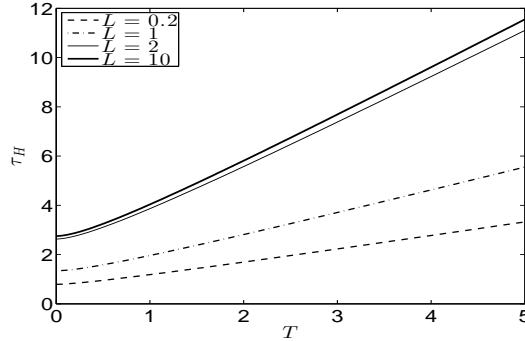


Fig. 4.3: Plot of the HB threshold τ_H versus T for the 1-D finite-domain problem (4.9) on $|x| \leq L$ where $L = 0.2$ (dashed curve), $L = 1$ (dashed-dotted curve), $L = 2$ (solid curve), and $L = 10$ (heavy solid curve). The threshold was computed numerically from (2.6) with $\chi(\tau\lambda)$ as given in (4.10). The one-spike solution is linearly stable when $\tau < \tau_H$. The threshold for $L = 10$ closely approximates that for the infinite-line problem, which was given in the left panel of Fig. 4.2.

We then set $\lambda = i\lambda_{IH}$ and numerically compute the roots of $g(i\lambda_{IH}) = 0$ using a Newton iteration scheme, where $g(\lambda)$ is defined in (2.6) in terms of χ as given in (4.10). The resulting HB curves τ_H versus T for four values of L are shown in Fig. 4.3. As L increases we see there is a wider range of τ at a given delay T where a one-spike solution is linearly stable.

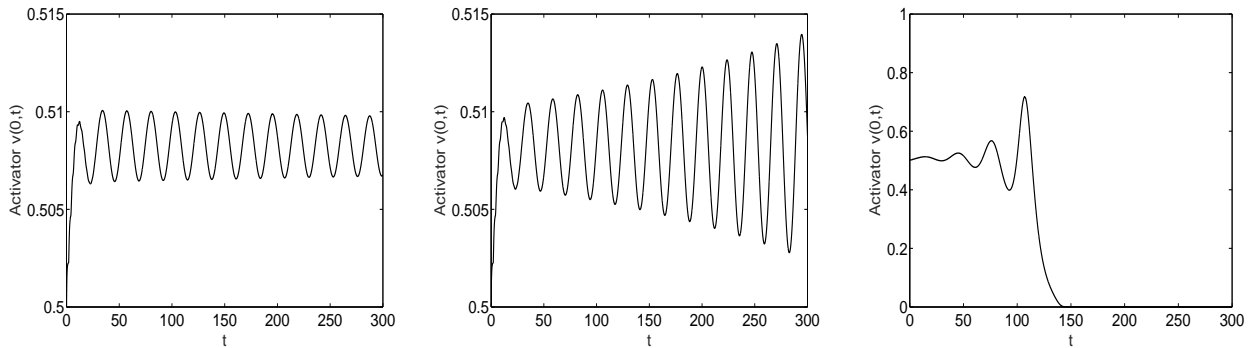


Fig. 4.4: Plot of the amplitude $v(0,t)$ of the spike versus t for $\tau = 5.3$ (left panel), $\tau = 5.6$ (middle panel), and $\tau = 10$ (right panel), as computed numerically by discretizing (4.9) with 151 spatial meshpoints on $[-2, 2]$ with $\epsilon = 0.05$ and $T = 2$. The theoretical HB prediction is $\tau_H \approx 5.573$ (see Fig. 4.3 with $L = 2$ and $T = 2$). The numerics shows a slowly decaying (growing) oscillation when $\tau = 5.3$ ($\tau = 5.6$), respectively. A large oscillation leading to a collapse of the spike occurs when τ is well-above the HB threshold (right panel).

As a partial verification of the results of Fig. 4.3 for the HB stability threshold, we took $\epsilon = 0.05$, $L = 2$, and $T = 2$, and discretized (4.9) with 151 spatial meshpoints using a method of lines approach. We then used the `dde23` solver of MATLAB to solve the system of delay (ordinary) differential equations (DDEs) for a value of τ slightly below and then slightly above the theoretically predicted HB threshold of $\tau_H \approx 5.573$. The numerical results shown in the left and middle panels of Fig. 4.4 confirm our prediction of the HB threshold. In the right panel of Fig. 4.4 we show that the spike amplitude first oscillates and then collapses for a value of τ that is considerably above the HB threshold.

5. The 2-D NLEP Problem: Computations and a Scaling Law. In this section we study the NLEP (2.7) characterizing the linear stability of an M -spot pattern, with $M \geq 2$, for the GM model (1.1) with delayed activator kinetics in a bounded 2-D domain. For both the synchronous and asynchronous modes of instability, we will show that a

time-delay in the activator kinetics leads to a wider parameter range where spot patterns are linearly stable.

5.1. The Synchronous Mode. We first consider the NLEP (2.7) for the synchronous mode by determining a parameterization of the HB curve in the τ versus β plane for a fixed delay $T \geq 0$. We substitute χ for the synchronous mode, as given in (2.7b), into (2.8) and set $\lambda = i\lambda_I$, with $\lambda_I \geq 0$, to obtain that

$$\frac{(1 + \beta)}{2} e^{i\lambda_I T} \left(\frac{1 + i\tau\lambda_I}{1 + \beta + i\tau\lambda_I} \right) = \mathcal{F}_\mu(i\lambda_I). \quad (5.1)$$

We solve this equation for β to get

$$\beta = -1 + \frac{2i\tau\lambda_I \mathcal{F}_\mu(i\lambda_I)}{e^{i\lambda_I T} (1 + i\tau\lambda_I) - 2\mathcal{F}_\mu(i\lambda_I)}, \quad (5.2)$$

and, upon taking the imaginary part of this expression, we conclude that

$$\text{Im} \left(\frac{2i\tau\lambda_I \mathcal{F}_\mu(i\lambda_I)}{e^{i\lambda_I T} (1 + i\tau\lambda_I) - 2\mathcal{F}_\mu(i\lambda_I)} \right) = 0. \quad (5.3)$$

We then separate $\mathcal{F}_\mu(i\lambda_I)$ into real and imaginary parts as

$$\mathcal{F}_\mu(i\lambda_I) = \mathcal{F}_{R\mu}(\lambda_I) + i\mathcal{F}_{I\mu}(\lambda_I). \quad (5.4)$$

Upon substituting (5.4) into (5.3), we solve for $\tau = \tau_H(\lambda_I)$ to obtain the parameterization

$$\tau_H = \frac{2|\mathcal{F}_\mu|^2 - \mathcal{F}_{R\mu} \cos(\lambda_I T) - \mathcal{F}_{I\mu} \sin(\lambda_I T)}{\lambda_I (\mathcal{F}_{I\mu} \cos(\lambda_I T) - \mathcal{F}_{R\mu} \sin(\lambda_I T))}, \quad (5.5)$$

where $\mathcal{F}_{R\mu} \equiv \mathcal{F}_{R\mu}(\lambda_I)$, $\mathcal{F}_{I\mu} \equiv \mathcal{F}_{I\mu}(\lambda_I)$, and $|\mathcal{F}_\mu| \equiv \sqrt{\mathcal{F}_{R\mu}^2 + \mathcal{F}_{I\mu}^2}$.

Similarly, if we solve (5.1) for $i\tau\lambda_I$, we get

$$i\tau\lambda_I = (1 + \beta) \left(\frac{2\mathcal{F}_\mu(i\lambda_I) - e^{i\lambda_I T}}{e^{i\lambda_I T} (1 + \beta) - 2\mathcal{F}_\mu(i\lambda_I)} \right). \quad (5.6)$$

By setting the real part of the right-hand side of (5.6) to zero, and upon solving the resulting equation for β , we obtain the parameterization $\beta = \beta_H(\lambda_I)$ where

$$\beta_H = \frac{4|\mathcal{F}_\mu|^2 + 1 - 4\mathcal{F}_{R\mu} \cos(\lambda_I T) - 4\mathcal{F}_{I\mu} \sin(\lambda_I T)}{2\mathcal{F}_{R\mu} \cos(\lambda_I T) + 2\mathcal{F}_{I\mu} \sin(\lambda_I T) - 1}. \quad (5.7)$$

The expressions (5.5) and (5.7) parametrize the HB threshold in the τ versus β plane in terms of $\lambda_I > 0$, at a fixed value of the delay T . We remark that if we replace \mathcal{F}_μ with \mathcal{F}_1 , corresponding to setting $T = 0$ in (5.5) and (5.7), we recover the parameterization given in equation (4.16) of [6] (see also Fig. 4.1 of [6]) for the 2-D GM model with no activator or inhibitor delays.

To implement (5.5) and (5.7) numerically, we write $\mathcal{F}_\mu(i\lambda_I)$ in terms of the complex-valued $\psi \equiv (L_\mu - i\lambda_I)^{-1}w^2$ as

$$\mathcal{F}_\mu(i\lambda_I) = \frac{\int_0^\infty \rho w \psi d\rho}{\int_0^\infty \rho w^2 d\rho}, \quad \text{where} \quad \Delta_\rho \psi - \psi + 2w (\cos(\lambda_I T) - i \sin(\lambda_I T)) \psi - i\lambda_I \psi = w^2, \quad (5.8)$$

where $w(\rho) > 0$ is the ground-state solution satisfying $\Delta_\rho w - w + w^2 = 0$. We solve for the ground-state numerically and then determine $\psi = \psi_R + i\psi_I$ from a BVP solver applied to ψ . In this way, we can readily compute $\mathcal{F}_{R\mu}(\lambda_I)$ and $\mathcal{F}_{I\mu}(\lambda_I)$ from (5.8), which is needed in our expressions (5.5) and (5.7) for the HB threshold.

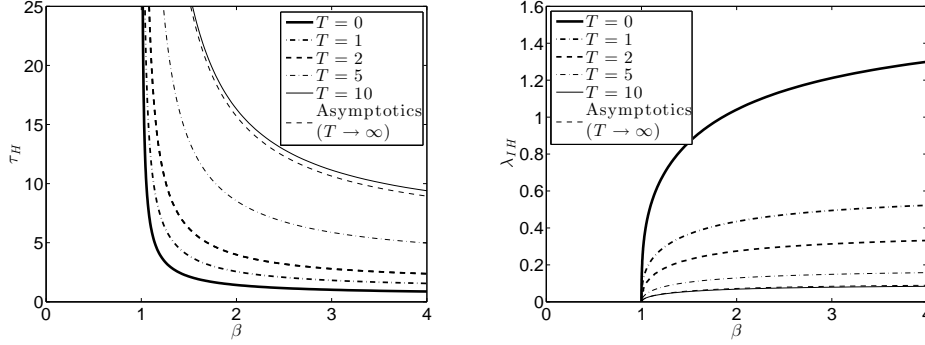


Fig. 5.1: HB thresholds for the synchronous mode computed from (5.5) and (5.7). Left panel: The HB threshold τ_H versus β for $T = 0$ (heavy solid curve). The spot pattern is linearly stable for all $\beta < 1$ and for $\tau < \tau_H$ when $\beta > 1$. From bottom to top, the various dashed curves are HB thresholds for $T = 1, T = 2, T = 5$ and $T = 10$. The thin solid curve is the asymptotic scaling law (5.12) for τ_H when $T = 10$. The effect of activator delay leads to a wider parameter range for stability. Right panel: plot of the HB frequency λ_{IH} versus β on $\beta > 1$ with the same labeling as in the left panel, except that now as λ_{IH} decreases as T increases. The thin solid curve is the asymptotic scaling law (5.12) for λ_{IH} when $T = 10$.

With this numerical approach, in the left panel of Fig. 5.1 we plot the HB threshold in the τ versus β plane for $T = 0$ and four nonzero values of the delay. The corresponding HB frequency, λ_{IH} , is plotted versus β in the right panel of Fig. 5.1. From this figure, we observe that a HB exists only on the range $\beta > 1$, and that $\tau_H \rightarrow +\infty$ as $\beta \rightarrow 1^+$. We also observe that at a fixed $\beta > 1$, τ_H increases as T increases, so that the effect of delayed activator kinetics is to increase the parameter range for the linear stability of the multi-spot pattern.

To determine the limiting behavior of τ_H for $T \gg 1$ at a fixed $\beta > 1$, we pose the scaling law $\tau_H \sim \tau_0 T$, $\lambda \sim ic_0/T$ where $c_0 > 0$ and $\tau_0 > 0$ are to be found. Upon substituting this into (3.1) we get

$$\Delta_\rho \Phi - \Phi + 2w [e^{-ic_0} + \dots] \Phi - [\chi_0 e^{-ic_0} + \dots] w^2 \int_0^\infty \frac{w \Phi \rho d\rho}{w^2 \rho d\rho} = \left[\frac{ic_0}{T} + \dots \right] \Phi, \quad (5.9)$$

where $\chi_0 = \chi(ic_0 \tau_0)$ is given in (2.7b). Setting $\Phi = w + \mathcal{O}(T^{-1})$, and using $\Delta_\rho w - w + w^2 = 0$, we get $-1 + (2 - \chi_0)e^{-ic_0} = 0$. This yields that

$$e^{ic_0} = 2 - \frac{2}{1 + \beta} \left(\frac{1 + \beta + i\tau_0 c_0}{1 + i\tau_0 c_0} \right) = \frac{2\beta}{1 + \beta} \left(\frac{i\tau_0 c_0}{1 + i\tau_0 c_0} \right). \quad (5.10)$$

Upon taking the modulus of (5.10), and solving for $\tau_0 c_0$, we get

$$\tau_0 c_0 = \frac{1}{\sqrt{f^2 - 1}}, \quad \text{where} \quad f \equiv \frac{2\beta}{1 + \beta}, \quad (5.11)$$

provided that $f > 1$, which implies that $\beta > 1$. Then, by taking the imaginary part of (5.10) we get

$$c_0 = \sin^{-1} \left(\frac{f\tau_0 c_0}{1 + \tau_0^2 c_0^2} \right).$$

In this way, we obtain for $\beta \equiv 2\pi MD_0/|\Omega| > 1$, that as $T \rightarrow +\infty$, there is a HB for the synchronous mode with the scaling law

$$\tau_H \sim \tau_0 T, \quad \tau_0 = \left(\frac{1}{\sqrt{f^2 - 1}} \right) \frac{1}{\sin^{-1}(\sqrt{f^2 - 1}/f)}, \quad f \equiv \frac{2\beta}{\beta + 1}, \quad (5.12a)$$

$$\lambda = i\lambda_{IH}, \quad \lambda_{IH} \sim c_0/T, \quad c_0 = \sin^{-1}(\sqrt{f^2 - 1}/f). \quad (5.12b)$$

We observe that for a fixed T with $T \gg 1$, we have $\tau_H \rightarrow +\infty$ and $\lambda_{IH} \rightarrow 0$ as $\beta \rightarrow 1^+$. A plot of the asymptotic results for λ_{IH} and τ_H versus β on $\beta > 1$ when $T = 10$ are shown in Fig. 5.1 to compare very well with full numerical results computed from the parameterization (5.5) and (5.7).

5.2. The Asynchronous Mode. We now consider the NLEP (2.7) for the asynchronous mode where $\chi = 2/(1 + \beta)$. We recall from Theorem 3.1 that there is a positive eigenvalue for any $T \geq 0$ when $\chi < 1$. Consequently, we conclude that the multi-spot pattern is unstable for any $T \geq 0$ when $\beta \equiv 2\pi MD_0/|\Omega| > 1$.

Next, we calculate the HB threshold in the T versus β plane, obtained by solving (2.8), which we write as a coupled system for $T = T_H$ and λ_{IH} , satisfying

$$\frac{(1 + \beta)}{2} \cos(\lambda_I T) = \mathcal{F}_{R\mu}(\lambda_I), \quad \frac{(1 + \beta)}{2} \sin(\lambda_I T) = \mathcal{F}_{I\mu}(\lambda_I), \quad (5.13)$$

where $\mathcal{F}_\mu(i\lambda_I) = \mathcal{F}_{R\mu}(\lambda_I) + i\mathcal{F}_{I\mu}(\lambda_I)$. This system is solved as β is varied by using Newton iterations. As a starting point, we let $\beta \gg 1$ and choose the minimum value T_H^1 of the delay for which L_μ has a pure imaginary eigenvalue $i\lambda_{IH}$. We then numerically path-follow this HB point as β is decreased. With this numerical approach, the HB threshold value of T_H and frequency λ_{IH} as a function of β are shown in the left and right panels of Fig. 5.2. From this figure, we observe that a HB occurs only when $\beta > 1$, and that $\lambda_{IH} \rightarrow 0^+$ and $T_H \rightarrow +\infty$ as $\beta \rightarrow 1^+$. For $\beta < 1$ the NLEP (2.7) for the asynchronous mode does not have a HB for any $T \geq 0$. Although there is a HB value of T when $\beta > 1$, the entire region $\beta > 1$ is linearly unstable for any $T \geq 0$, as the NLEP always has a positive real eigenvalue. In contrast, when $\beta < 1$, we conclude that $\text{Re}(\lambda) \leq 0$ for any $T \geq 0$.

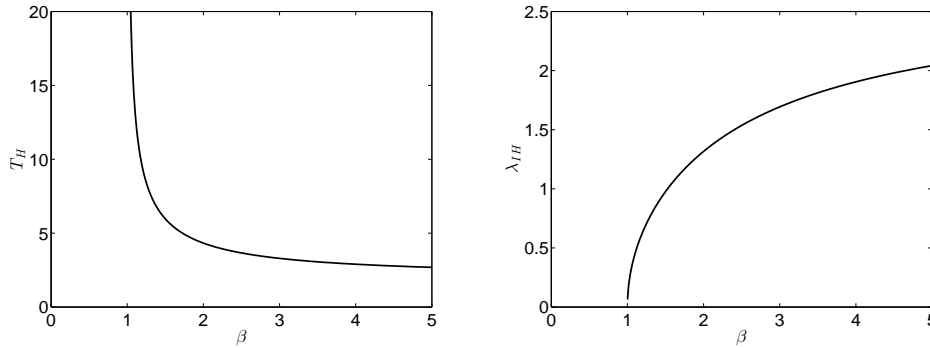


Fig. 5.2: HB threshold for the asynchronous mode computed from (5.13). Left panel: The minimum value T_H of T versus β where a HB occurs. Right panel: The HB frequency λ_{IH} versus β . We observe that a HB occurs only on $\beta > 1$ with $\lambda_{IH} \rightarrow 0^+$ and $T_H \rightarrow +\infty$ as $\beta \rightarrow 1^+$. For $\beta > 1$ the NLEP (2.7) for the asynchronous mode also has a positive real eigenvalue for any $T \geq 0$. When $\beta < 1$, we predict that the multi-spot pattern is linearly stable for any $T \geq 0$.

Finally, we compare our HB threshold for the asynchronous mode with only activator delay with corresponding thresholds for the case of both activator and inhibitor delay, and with only inhibitor delay. In the former case v_T^2/u in (1.1) is replaced with v_T^2/u_T , whereas when there is only inhibitor delay v_T^2/u and $\varepsilon^{-N}v_T^2$ in (1.1) are replaced with v^2/u_T and $\varepsilon^{-N}v^2$. When there is both activator and inhibitor delay, $\chi\mu$ in (2.7) is replaced with $\chi\mu^2$, and a HB of the NLEP must be a root $\lambda_I = \lambda_{IH}$ and $T = T_H$ of the coupled system

$$\frac{(1 + \beta)}{2} \cos(2\lambda_I T) = \mathcal{F}_{R\mu}(\lambda_I), \quad \frac{(1 + \beta)}{2} \sin(2\lambda_I T) = \mathcal{F}_{I\mu}(\lambda_I), \quad (5.14)$$

In contrast, when there is only inhibitor delay, L_μ in (2.7) is replaced by its undelayed counterpart $L_1\Phi \equiv \Delta_\rho\Phi - \Phi + 2w\Phi$,

and a HB of the NLEP must be a root of

$$\frac{(1+\beta)}{2} \cos(\lambda_I T) = \mathcal{F}_{R1}(\lambda_I), \quad \frac{(1+\beta)}{2} \sin(\lambda_I T) = \mathcal{F}_{I1}(\lambda_I), \quad (5.15)$$

where $\mathcal{F}_1(i\lambda_I) = \mathcal{F}_{R1}(\lambda_I) + i\mathcal{F}_{I1}(\lambda_I)$ now depends only on λ_I and not T . As a result, in this latter case, we can conveniently parameterize the HB in the T versus β plane in terms of λ_I as

$$\beta = 2\sqrt{|\mathcal{F}_1(i\lambda_I)|^2 - 1}, \quad T_H = \frac{1}{\lambda_I} \tan^{-1} \left(\frac{\mathcal{F}_{I1}(\lambda_I)}{\mathcal{F}_{R1}(\lambda_I)} \right). \quad (5.16)$$

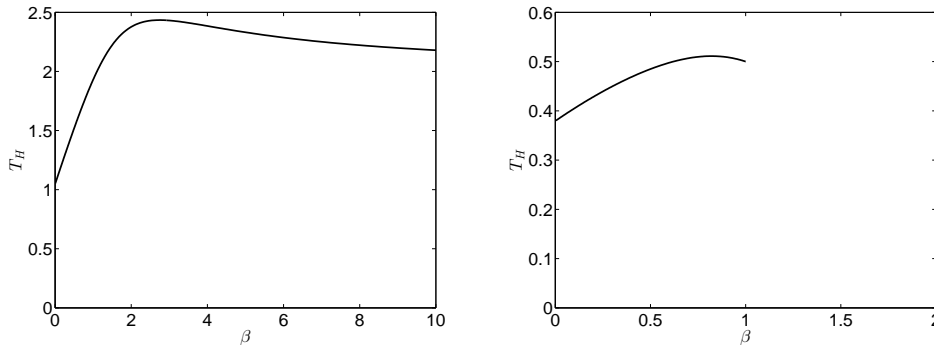


Fig. 5.3: Left panel: The minimum value T_H of T versus β where a HB occurs when the time delay occurs for both the activator and inhibitor kinetics, as computed numerically from (5.14). The HB threshold occurs for any $\beta > 0$. Right panel: The corresponding HB threshold when the time-delay occurs only for the inhibitor, as computed numerically from the parameterization (5.16). The HB threshold only occurs on $0 < \beta < 1$, and $T_H \rightarrow 1/2$ with $\lambda_{IH} \rightarrow 0^+$ as $\beta \rightarrow 1^-$.

By solving (5.14) using Newton's method, and by using the parameterization (5.16), in the left and right panels of Fig. 5.3 we plot the minimum value T_H of the delay for which a HB occurs. In comparison with the left panel of Fig. 5.2 for the case of only activator delay, we observe from the left panel of Fig. 5.3 that when there is both activator and inhibitor delay there is a HB for the entire range $\beta > 0$. For the range $\beta > 1$, the HB value of T with both activator and inhibitor delay is smaller than that with only activator delay. Moreover, when there is only inhibitor delay, as shown in the right panel of Fig. 5.3 we observe that there is a HB only on the range $0 < \beta < 1$, and on this range the HB threshold in T is smaller than with both activator and inhibitor delay. This HB branch terminates as $\beta \rightarrow 1^-$, owing to the fact that $\lambda_{IH} \rightarrow 0^+$ as $\beta \rightarrow 1^-$. Since $\mathcal{F}_{I1}(\lambda_I) \sim \lambda_I/2$ as $\lambda_I \rightarrow 0^+$ and $\mathcal{F}_{R1}(0) = 1$ (see [22]), we readily calculate from (5.16) that $T_H \rightarrow 1/2$ as $\beta \rightarrow 1^-$. This confirms the limiting value shown in the right panel of Fig. 5.3.

In summary, we conclude that when there is only delayed activator kinetics the multi-spot pattern is linearly stable to asynchronous perturbations in the amplitudes of the spots for any delay $T \geq 0$ when $\beta \equiv 2\pi MD_0/|\Omega| < 1$. If there is any inhibitor delay, then there is a HB stability threshold in T on the range $0 < \beta < 1$. In this sense, delayed activator kinetics leads to better stability properties than when inhibitor delay is included.

6. Discussion. We have studied the onset of an oscillatory instability in the amplitude of a localized spike solution for various limiting forms of the GM activator-inhibitor RD model in the case where the nonlinear activator kinetics has a fixed time-delay. Such an instability arises from a Hopf bifurcation associated with a new class of nonlocal eigenvalue problem (NLEP). The motivation for the study of this problem is the previous computational studies (cf. [7], [15], [16], [18]) of pattern formation in RD systems with a fixed time-delay in the reaction kinetics, which models time lags needed for the expression of genes. In contrast to the conclusion of our recent analysis of [6], where a time-delay was assumed in

both the activator and inhibitor kinetics, we showed herein that a time-delay in only the activator kinetics has a *stabilizing* effect, in the sense that there is a larger region in parameter space where a spike solution is linearly stable than when there is no delayed reaction kinetics. Phase diagrams exhibiting these larger parameter regions where the spike is linearly stable under the effect of delayed activator kinetics were generated from a numerical study of the NLEP, together with analytical scaling laws for the Hopf bifurcation thresholds in the limit of large delay.

We now briefly discuss a few possible additional directions that warrant further study. Firstly, from a modeling viewpoint, although we have considered only the effect of delayed activator kinetics on the GM model, the present study suggests more generally that, when there is a time-delay in only the autocatalytic term in the reaction kinetics, localized RD patterns will have similar enhanced stability properties. It would be interesting to study this conjecture for other choices of the reaction kinetics and, more importantly, to try to develop realistic biological modeling scenarios for which it is only the autocatalytic component of the nonlinearity that undergoes a fixed time-delay.

From a mathematical viewpoint, our analysis has only considered the linear stability of spike solutions on an $\mathcal{O}(1)$ time-scale, as characterized by the spectrum of an NLEP. For the 1-D finite-domain problem, it would be interesting to extend our analysis to study the effect of a time-delay in the activator kinetics on the small eigenvalue of order $\mathcal{O}(\epsilon^2)$ (cf. [11]) in the linearization of a one-spike steady-state pattern. A Hopf bifurcation for this small eigenvalue as the activator delay increases would lead to a small-amplitude oscillatory motion in the spatial location of the spike. To study large-scale motion in the location of a spike, one would have to derive and then analyze a delay differential ordinary differential equation for the location of a spike. With no delayed reaction kinetics, such an analysis was given in [12].

Finally, we remark on a possible interesting effect of delayed activator kinetics on the linear stability of homoclinic stripe patterns in bounded 2-D domains. For the GM model, such homoclinic stripe solutions, formed from the localization of a spike on a one-dimensional curve in a 2-D domain, are known to be unconditionally unstable to breakup into localized spots unless one includes a strong saturation mechanism for the autocatalysis term (cf. [14], [19]). As the saturation parameter increases towards a critical value associated with a homoclinic bifurcation point, it has been shown that the principal eigenvalue of the local part of the linearized operator decreases to zero. This mechanism has been shown for straight stripes in [14], and more generally in [19], to eliminate the band of unstable breakup modes associated with the underlying NLEP, leading to a stabilization of the homoclinic stripe. Since the effect of increasing the time-delay in the activator kinetics also decreases the principal eigenvalue of the local part of the linearized operator to zero (see the left panel of Fig. 3.1), we anticipate that a homoclinic stripe solution will be linearly stable to breakup instabilities whenever the time-delay is large enough. It would be interesting to examine in detail this new conjectured mechanism to stabilize homoclinic stripes in 2-D domains.

Acknowledgements. M. J. Ward and J. Wei were supported by NSERC (Canada).

Appendix A. The Delayed Local Operator in 1-D: An Explicit Formula.

We determine the spectrum of the delayed local operator (3.3) in 1-D, written for $\Phi = \Phi(y)$ as

$$\Phi'' - \Phi + 2\mu w\Phi = \lambda\Phi, \quad \Phi \in H^1(\mathbb{R}^1), \quad \text{where } \mu = e^{-\lambda T}, \quad w(y) = \frac{3}{2}\text{sech}^2(y/2). \quad (\text{A.1})$$

To determine the spectrum, we first convert this problem into a standard problem for hypergeometric functions by following a similar approach done in [4]. As in [4], we introduce the new variables γ and $\phi(y)$ by

$$\gamma \equiv \sqrt{1 + \lambda}, \quad \Phi = w^\gamma \phi, \quad (\text{A.2})$$

and specify the principal branch of $\sqrt{1 + \lambda}$ so that $\text{Re}(\gamma) > 0$. Then, upon using $w'' = w - w^2$ and $(w')^2 = w^2 - 2w^3/3$,

a simple calculation shows that

$$\phi'' + 2\gamma \frac{w'}{w} \phi' + \left(2\mu - \gamma - \frac{2}{3}\gamma(\gamma - 1)\right) w\phi = 0. \quad (\text{A.3})$$

Next we introduce the new independent variable z , defined by

$$z = \frac{1}{2} \left(1 - \frac{w'}{w}\right). \quad (\text{A.4})$$

Upon using $w \sim e^{-|y|}$ as $y \rightarrow \pm\infty$ and the monotonicity of w'/w , (A.4) provides a one-to-one map of $-\infty < y < \infty$ to $0 < z < 1$. We calculate that

$$\frac{dz}{dy} = -\frac{1}{2} \left(\frac{w''}{w} - \frac{(w')^2}{w^2}\right) = -\frac{1}{2} \left(\frac{w - w^2}{w} - \frac{(w^2 - 2w^3/3)}{w^2}\right) = \frac{w}{6}.$$

We have $z'' = w'/6$ so that $w'/w = z''/z'$. Using $w'/w = 1 - 2z$ from (A.4), we obtain that $z'' = z' - 2zz'$. Upon integrating this expression once we get that

$$\frac{dz}{dy} = z(1 - z), \quad w = 6z(1 - z). \quad (\text{A.5})$$

As such, if we define $\mathcal{Y}(z) = \phi[y(z)]$, we readily calculate from (A.3) and (A.5) that $\mathcal{Y}(z)$ satisfies the hypergeometric differential equation

$$z(1 - z)\mathcal{Y}'' + (c - (a + b + 1)z)\mathcal{Y}' - ab\mathcal{Y} = 0, \quad (\text{A.6a})$$

where the coefficients a, b, c are

$$a + b + 1 = 4\gamma + 2, \quad ab = 4\gamma(\gamma - 1) + 6\gamma - 12\mu, \quad c = 1 + 2\gamma, \quad \text{where} \quad \gamma = \sqrt{1 + \lambda}. \quad (\text{A.6b})$$

The general solution to (A.6a), in terms of arbitrary constants d_1 and d_2 , can be written in terms of standard hypergeometric functions as (cf. [20])

$$\mathcal{Y}(z) = d_1 F(a, b; c; z) + d_2 z^{1-c} F(a - c + 1, b - c + 1; 2 - c; z). \quad (\text{A.7})$$

As $z \rightarrow 0$, corresponding to $y \rightarrow -\infty$, we have upon using (A.6b) that $\mathcal{Y}(z) = \mathcal{O}(z^{-2\gamma}) \rightarrow +\infty$ unless $d_2 = 0$. Then, since $w = \mathcal{O}(z)$ as $z \rightarrow 0$ from (A.5), we use (A.2) to get $\Phi = \mathcal{O}(w^{-\gamma})$ as $y \rightarrow -\infty$ unless $d_2 = 0$. Therefore, since $\text{Re}\gamma > 0$, a necessary condition for $\Phi \in H^1(\mathbb{R}^1)$ is that $d_2 = 0$ in (A.7).

Next, using (A.6b) we calculate $\text{Re}(a + b - c) = 2\text{Re}\gamma > 0$ by our choice of branch cut. Therefore, from [20] we have that $F(a, b; c; z)$ has the following singular behavior as $z \rightarrow 1$ in terms of the Gamma function $\Gamma(x)$:

$$F(a, b; c; z) \sim \frac{\Gamma(c)\Gamma(a + b - c)}{z^{c-a-b}\Gamma(a)\Gamma(b)}, \quad \text{as } z \rightarrow 1, \quad (\text{A.8})$$

so that $\Phi(y) = w^\gamma \mathcal{Y}(z(y)) = \mathcal{O}(w^{-\gamma})$ as $y \rightarrow \infty$. To eliminate this possible singular behavior as $y \rightarrow +\infty$, we must choose a, b and c to eliminate the coefficient of the singularity in (A.8). Since $\text{Re}(c) > 0$ and $\text{Re}(a + b - c) > 0$, we conclude that Φ is regular as $y \rightarrow +\infty$ iff $\Gamma(x)$ has a pole at a or b . In other words iff $a, b = 0, -1, -2, \dots$. With this criterion, and using (A.6b), we compute that $a = 2\gamma - \alpha$ and $b = 2\gamma + 1 + \alpha$, where α is one of the two roots of the quadratic

$$\alpha^2 + \alpha - 12\mu = 0. \quad (\text{A.9})$$

Since the two roots satisfy $\alpha_+ + \alpha_- = 1$, where $\text{Re}(\alpha_+) > 0$ and $\text{Re}(\alpha_-) < 0$, then $\Gamma(x)$ has a pole at a or b iff $2\gamma - \alpha_+ = -l$ with $l = 0, 1, 2, \dots$. With α_+ being the root of (A.9) for which $\text{Re}(\alpha_+) > 0$, we conclude that $\Phi \in H^1(\mathbb{R})$ iff

$$2\gamma - \alpha_+ = -l, \quad l = 0, 1, 2, \dots \quad (\text{A.10})$$

By solving for α_+ and letting $\mu = e^{-\lambda T}$, (A.10) yields a family of transcendental equations parametrized by l , as written in (3.4) of §3.1. Real-valued roots of (A.10), corresponding to real eigenvalues of L_μ , are analyzed in §3.1.

Next, we examine whether (A.10) admits a pure imaginary eigenvalue $\lambda = i\lambda_I$, where without loss of generality we take $\lambda_I > 0$. Our goal is to derive the explicit characterization (3.7)–(3.9) given in §3.1. We first write $\alpha_+ = \alpha_R + i\alpha_I$, and obtain from (A.10) that

$$2\text{Re}\gamma - \alpha_R = -l, \quad 2\text{Im}\gamma - \alpha_I = 0. \quad (\text{A.11})$$

Since $\gamma = \sqrt{1 + i\lambda_I}$, this yields

$$(\alpha_R - l)^2 - \alpha_I^2 = 4 [(\text{Re}\gamma)^2 - (\text{Im}\gamma)^2] = 1, \quad (\text{A.12})$$

which implies that $\alpha_R \geq l + 2$. Next, we separate (A.9) into real and imaginary parts, using $\mu = \mu_R + i\mu_I$, which yields

$$\alpha_R^2 + \alpha_R - \alpha_I^2 = 12\mu_R, \quad \alpha_I(2\alpha_R + 1) = 12\mu_I; \quad \mu_R = \cos(\lambda_I T), \quad \mu_I = -\sin(\lambda_I T). \quad (\text{A.13})$$

We combine (A.12) with the first of (A.13), and solve the resulting expression for α_R to get

$$\alpha_R = \frac{l^2 - 4 + 12\mu_R}{1 + 2l}. \quad (\text{A.14})$$

Since $\alpha_R \geq l + 2$, (A.14) implies that l must satisfy $(l+1)(l+5) \leq 12\mu_R$. Since $-1 < \mu_R < 1$, we obtain the key conclusion that $l = 0$ and $l = 1$ are the only possible choices in (A.10) that admit a pure complex eigenvalue $\lambda = i\lambda_I$. Since $l = 1$ corresponds trivially to $\lambda_I = 0$ for all $T \geq 0$, $l = 0$ is the only choice leading to $\lambda_I > 0$.

With $l = 0$, we get α_R from (A.14) and α_I from the second equation of (A.13). This yields that

$$\alpha_R = -4 + 12\mu_R, \quad \alpha_I = \frac{12\mu_I}{1 + 2\alpha_R}, \quad \alpha_R + i\alpha_I = 2\text{Re}(\sqrt{1 + i\lambda_I}) + 2i\text{Im}(\sqrt{1 + i\lambda_I}). \quad (\text{A.15})$$

These expressions, which relate λ_I to μ , show that we must have $\mu_R = \cos(\lambda_I T) > 1/2$ and $\mu_I = -\sin(\lambda_I T) > 0$ when $\lambda_I > 0$. Finally, we substitute (A.15) into the first equation of (A.13) to obtain, after some algebra, that

$$(24\mu_R - 7)^2 (12\mu_R^2 - 8\mu_R + 1) - 12\mu_I^2 = 0. \quad (\text{A.16})$$

Upon labeling $\theta \equiv \lambda_I T$, we conclude that θ must be a root of $\mathcal{H}(\theta) = 0$, where

$$\mathcal{H}(\theta) \equiv (24 \cos \theta - 7)^2 (12 \cos^2 \theta - 8 \cos \theta + 1) - 12 \sin^2 \theta, \quad (\text{A.17})$$

for which $\cos \theta > 1/2$ and $\sin \theta < 0$. We use $\mathcal{H}(\theta) = \mathcal{H}(-\theta)$, $\mathcal{H}(0) > 0$, $\mathcal{H}(\pi/3) < 0$, and $\mathcal{H}(\theta)$ is monotonically increasing on $0 < \theta < \pi/3$ to obtain the sequence of values $\theta_n = \theta_0 + 2\pi n$ with $n = 1, 2, 3, \dots$ where a pure complex eigenvalue occurs. Here $\theta_0 < 0$ is the unique root to $\mathcal{H}(\theta) = 0$ in $-\pi/3 < \theta < 0$. This yields (3.7) and (3.9) as written in §3.1.

Finally, to obtain λ_I , as written in (3.8), we set $\theta = \lambda_I T$, we use $4\sqrt{1 + i\lambda_I} + 1 = \sqrt{1 + 48(\cos \theta_n - i \sin \theta_n)}$, where $\theta_n = -\theta_0 + 2\pi n$. Upon squaring both sides and taking the imaginary parts of the resulting expression we obtain (3.8) for λ_I , which is independent of n . This completes the derivation of (3.7)–(3.9), which determines all values of the delay T for which L_μ has purely imaginary eigenvalues in one space dimension.

REFERENCES

- [1] S. Chen, J. Shi, *Global attractivity of equilibrium in Gierer-Meinhardt system with activator production saturation and gene expression time delays*, Nonlinear Analysis: Real World Applic., **14**(4), (2013), pp. 1871–1886.
- [2] S. Chen, J. Shi, J. Wei, *Time delay-induced instabilities and Hopf bifurcations in general reaction-diffusion systems*, J. Nonl. Sci., **23**(1), (2013), pp. 1–38.
- [3] E. N. Dancer, *On stability and Hopf bifurcations for chemotaxis systems*, Meth. Applic. of Anal., **8**(2), (2001), pp. 245–256.
- [4] A. Doelman, A. Gardner, T. J. Kaper, *Stability analysis of singular patterns in the 1-D Gray-Scott model: A matched asymptotic approach*, Physica D, **122**(1-4), (1998), pp. 1–36.
- [5] A. Doelman, R. A. Gardner, T. Kaper, *Large stable pulse solutions in reaction-diffusion equations*, Indiana U. Math. Journ., **50**(1), (2001), pp. 443–507.
- [6] N. T. Fadai, M. J. Ward, J. Wei, *Delayed reaction-kinetics and the stability of spikes in the Gierer-Meinhardt Model*, SIAM J. Appl. Math., to appear, (2016), (27 pages).
- [7] E. A. Gaffney, N. A. M. Monk, *Gene expression time delays and Turing pattern formation systems*, Bull. Math. Bio., **68**, (2006), pp. 99–130.
- [8] A. Gierer, H. Meinhardt, *A theory of biological pattern formation*, Kybernetik, **12**, (1972), pp. 30–39.
- [9] I. Gokhberg, M. Krein, *Fundamental theorems on deficiency indices, root numbers and indices of linear operators*, Amer Math Soc. Transl., **2**(13), (1960), pp. 185–264.
- [10] D. Iron, M. J. Ward, *A metastable spike solution for a non-local reaction-diffusion model*, SIAM J. Appl. Math., **60**(3), (2000), pp. 778–802.
- [11] D. Iron, M. J. Ward and J. Wei, *The stability of spike solutions to the one-dimensional Gierer-Meinhardt model*, Physica D, **150**(1-2), (2001), pp. 25–62.
- [12] D. Iron, M. J. Ward, *The dynamics of multi-spike solutions for the one-dimensional Gierer-Meinhardt model*, SIAM J. Appl. Math., **62**(6), (2002), pp. 1924–1951.
- [13] T. Kato, *Perturbation theory for linear operators*, second edition, Springer-Verlag, Berlin, 1976.
- [14] T. Kolokolnikov, W. Sun, M. J. Ward, J. Wei, *The stability of a stripe for the Gierer-Meinhardt model and the effect of saturation*, SIAM J. Appl. Dyn. Sys., **5**(2), (2006), pp. 313–363.
- [15] S. Lee, E. A. Gaffney, N. A. M. Monk, *The influence of gene expression time delays on Gierer-Meinhardt pattern formation systems*, Bull. Math. Bio., **72**(8), (2010), pp. 2139–2160.
- [16] S. Lee, E. A. Gaffney, *Aberrant behaviors of reaction-diffusion self-organization models on growing domains in the presence of gene expression time delays*, Bull. Math. Bio., **72**(8), (2010), pp. 2161–2179.
- [17] S. Lee, E. A. Gaffney, R. E. Baker, *The dynamics of Turing patterns for morphogen-regulated growing domains with cellular response delays*, Bull. Math. Bio., **73**, (2011), pp. 2527–2551.
- [18] P. Maini, T. Woolley, R. E. Baker, E. A. Gaffney, S. Lee, *Turing’s model for biological pattern formation and the robustness problem*, Interface Focus, **2012**(2), (2012), pp. 487–496.
- [19] I. Moyles, M. J. Ward, *Existence, stability, and dynamics of ring and near-ring Solutions to the Gierer-Meinhardt model in the semi-strong regime*, under revision, SIAM J. Appl. Dyn. Sys., (2016), (44 pages).
- [20] L. J. Slater, *Generalized hypergeometric functions*, Cambridge University Press, Cambridge, U.K., 1966.
- [21] A. Turing, *The Chemical Basis of Morphogenesis*, Phil. Trans. Roy. Soc. B, **327**, (1952), pp. 37–72.
- [22] M. J. Ward, J. Wei, *Hopf bifurcation of spike solutions for the shadow Gierer-Meinhardt model*, Europ. J. Appl. Math., **14**(6), (2003), pp. 677–711.
- [23] M. J. Ward, J. Wei, *Hopf bifurcations and oscillatory instabilities of spike solutions for the one-dimensional Gierer-Meinhardt model*, J. Nonlinear Science, **13**(2), (2003), pp. 209–264.
- [24] J. Wei, *On single interior spike solutions for the Gierer-Meinhardt system: uniqueness and spectrum estimates*, Europ. J. Appl. Math., **10**(4), (1999), pp. 353–378.
- [25] J. Wei, M. Winter, *Critical threshold and stability of cluster solutions for large reaction-diffusion systems in \mathbb{R}^1* , SIAM J. Math. Anal., **33**(5), (2002), pp. 1058–1089.
- [26] J. Wei, M. Winter, *Spikes for the two-dimensional Gierer-Meinhardt system: the weak coupling case*, J. Nonlinear Sci., **11**(6), (2001), pp. 415–458.